JBC RESEARCH ARTICLE

Structural analyses of apolipoprotein A-IV polymorphisms Q360H and T347S elucidate the inhibitory effect against thrombosis

Received for publication, November 7, 2024, and in revised form, February 20, 2025 Published, Papers in Press, March 10, 2025,
https://doi.org/10.1016/j.jbc.2025.108392

Aron A. Shoara[1,2,3,4,5,6], **Sladjana Slavkovic**[2,3,7], **Miguel A. D. Neves**[2,3,7], **Preeti Bhoria**[2,6], **Viktor Prifti**[2,6,7], **Pingguo Chen**[2,3,6], **Logan W. Donaldson**[8], **Andrew N. Beckett**[1,2,3,4], **Philip E. Johnson**[9,*], **and Heyu Ni**[1,2,3,5,6,7,*]

From the [1]*Department of Medicine, University of Toronto, Toronto, Ontario, Canada;* [2]*Keenan Research Centre for Biomedical Science, Li Ka Shing Knowledge Institute, St Michael's Hospital, Toronto, Ontario, Canada;* [3]*Centre for Innovation, Canadian Blood Services, Toronto, Ontario, Canada;* [4]*Royal Canadian Medical Service, Canadian Armed Forces, Ottawa, Ontario, Canada;* [5]*Department of Physiology, University of Toronto, Toronto, Ontario, Canada;* [6]*Toronto Platelet Immunobiology Group, University of Toronto, Toronto, Ontario, Canada;* [7]*Department of Laboratory Medicine and Pathobiology, University of Toronto, Toronto, Ontario, Canada;* [8]*Department of Biology, and* [9]*Department of Chemistry, York University, Toronto, Ontario, Canada*

Reviewed by members of the JBC Editorial Board. Edited by George M. Carman

Apolipoprotein A-IV (apoA-IV) is an abundant lipid-binding protein in blood plasma. We previously reported that apoA-IV, as an endogenous inhibitor, competitively binds platelet αIIbβ3 integrin from its N-terminal residues, reducing the potential risk of thrombosis. This study aims to investigate how the apoA-IV^{Q360H} and apoA-IV^{T347S} mutations affect the structure and function of apoA-IV. These mutations are linked to increased risk of cardiovascular diseases because of multiple single-nucleotide polymorphisms in the C-terminal region of apoA-IV. We postulate that the structural hindrance caused by the C-terminal motifs may impede the binding of apoA-IV to platelets at its N-terminal binding site. However, the mechanistic impact of Q360H and T347S polymorphisms on this intermolecular interaction and their potential contribution to the development of cardiovascular disease have not been adequately investigated. To address this, recombinant forms of human apoA-IV^{WT}, apoA-IV^{Q360H}, and apoA-IV^{T347S} variants were produced, and the structural stability, dimerization, and molecular dynamics of the C terminus were examined utilizing biophysical techniques, including fluorescence anisotropy, fluorescence spectrophotometry, circular dichroism, and biolayer interferometry methods. Our results showed a decreased fraction of α-helix structure in apoA-IV^{Q360H} and apoA-IV^{T347S} compared with the WT, and the inhibitory effect of dimerized apoA-IV on platelet aggregation was reduced in apoA-IV^{Q360H} and apoA-IV^{T347S} variants. Binding kinetics of examined apoA-IV polymorphisms to platelet αIIbβ3 suggest a potential mechanism for increased risk of cardiovascular diseases in individuals with apoA-IV^{Q360H} and apoA-IV^{T347S} polymorphisms.

Apolipoprotein A-IV (apoA-IV) is a lipid-emulsifying protein in plasma that can be interchanged with other apolipoproteins (apoA-I, apoB, and apoE) (1, 2). Human apoA-IV is primarily synthesized in the intestine and plays important roles in lipid metabolism, reverse cholesterol transport, glucose homeostasis in plasma, and putative attenuation of thrombosis (2–7). ApoA-IV is reported to exhibit multiple 22-mer amphipathic structures of α-helix bundles and as low as 5% glycosylation (8–10). The gene encoding for human apoA-IV (apoA-IV-1 or apoA-IV^{WT}) is reported to have seven single-nucleotide polymorphisms (11, 12). The second most abundant apoA-IV polymorphism possesses an ACT to TCT variation at codon 347, which has an allele frequency of 0.22 to 0.25. This variant encodes a serine to threonine substitution (apoA-IV-1a or apoA-IV^{T347S}). The third most common apoA-IV polymorphism with an allele frequency of 0.03 to 0.12 has a CAG to CAT variation at codon 360, encoding a histidine for glutamine replacement (apoA-IV-2 or apoA-IV^{Q360H}) (12–14). While previous research examining the impact of heterozygous expression of apoA-IV polymorphisms found no significant differences compared with apoA-IV^{WT} (15), several epidemiological studies have documented that individuals carrying homozygous apoA-IV^{T347S} or apoA-IV^{Q360H} allele have an increased susceptibility to coronary heart disease, although the mechanisms behind this correlation have not been adequately explored (16–18).

Platelets, small anucleate cells in the blood, hold key functions in thrombosis and hemostasis (19–21). They also actively contribute to inflammation, immune responses, tumor metastasis, and atherosclerosis (22–26). Integrins are a conserved ubiquitous class of heterodimeric cell surface adhesion proteins. The predominant integrin on platelets is GPIIbIIIa (αIIbβ3), which is essential for platelet aggregation and important for platelet adhesion to the injured vessel wall (19, 24, 27–29). Platelet activation leads to the formation of a plug by crosslinking adjacent platelets through the interaction of integrin αIIbβ3 and fibrinogen (Fg), which can recruit

Statement of prior presentation: Some of the data in this article have been presented orally at the International Society of Thrombosis and Haemostasis, June 2023.

* For correspondence: Philip E. Johnson, pjohnson@yorku.ca; Heyu Ni, heyu.ni@unityhealth.to.

additional platelets, coagulation factors, and enhance blood coagulation (27–32). Classically, Fg has been identified as the molecule that mediates platelet aggregation; however, our earlier studies demonstrated that occlusive thrombi can still occur without either or both Fg and von Willebrand factor, suggesting the existence of yet unidentified molecules that bind to αIIbβ3 and contribute to platelet aggregation and thrombosis (28, 33–35). Prior studies on apoA-IV have shown that protein–protein interactions depend on a highly conserved N-terminal region, and lipid binding depends on key prolines (36, 37). In a recent study, we investigated the role of apoA-IV^{WT} in platelet activity and thrombosis, two important factors that contribute to heart attacks and strokes (4, 7, 20). This study revealed that apoA-IV is a novel ligand of αIIbβ3 *via* its highly conserved N-terminal region (E1–L38), and negatively charged aspartic acid residues (D5, D13) were potential αIIbβ3-binding sites (4). Also, other structural studies of apoA-IV showed the role of conserved proline residues in shaping the structure and the lipid-binding function of human apoA-IV. Our data demonstrated that apoA-IV is a novel ligand of αIIbβ3 *via* its highly conserved N-terminal region (E1-L38), and the negatively charged aspartic acid residues (D5, D13) were potential αIIbβ3-binding sites, which are critical for endogenous inhibition of thrombosis (4, 5). Furthermore, apoA-IV was able to attenuate platelet aggregation and activation *in vitro* and prevented thrombi *in vivo*. Finally, we demonstrated that circadian rhythms in humans were negatively correlated with platelet aggregation (4).

The present study aims to examine the impact of the three most common apoA-IV variants, namely apoA-IV^{WT}, apoA-IV^{T347S}, and apoA-IV^{Q360H}, on the structural and functional characteristics of this plasma protein and explored a hypothesis that an alteration in the structure of apoA-IV variants affects binding to platelet integrin αIIbβ3. The work provides evidence for why individuals with the apoA-IV^{Q360H} and apoA-IV^{T347S} polymorphisms are more susceptible to cardiovascular diseases, providing valuable insights for prevention. This work demonstrates the value of performing comprehensive biochemical studies to understand the role of apoA-IV polymorphisms in cardiovascular disease, platelet-related diseases, and inflammation as well as advancing therapies against these diseases.

Results

CD spectroscopy showed a change in helicity of apoA-IV polymorphisms

Human apoA-IV polymorphism (WT, T347S, and Q360H) proteins were expressed and purified as we described elsewhere (4). A series of structural studies on these variants were conducted utilizing circular dichroism (CD) spectroscopy to determine the α-helical content of apoA-IV variants (Figs. 1*A* and S1). ApoA-IV^{WT}, apoA-IV^{T347S}, and apoA-IV^{Q360H} polymorphisms exhibited two minima at 207 and 222 nm indicative of α-helical protein structure (Fig. 1*A*). The average α-helix contents (fractional helicity) of each variant were calculated and identified that apoA-IV^{T347S} had (48 ± 5)% α-helix content, whereas apoA-IV^{Q360H} and apoA-IV^{WT} contained (63 ± 5)% and (69 ± 2)% α-helix content, respectively. These differences in the α-helix content demonstrate significant reduction in the mean fractional helicity of apoA-IV^{T347S} polymorphism compared with that in apoA-IV^{WT} and apoA-IV^{Q360H} isoforms (Fig. 1*B*).

Protein folding stability studies revealed denaturation points for apoA-IV isoforms

To test the thermal stability of apoA-IV polymorphisms, we measured mean molar ellipticity, [Θ], at 222 nm in a temperature range of 25 to 75 °C (Fig. 1*C*). Using first derivative analyses of the obtained dichroic thermograms, we quantified thermal denaturation points (T_m) for apoA-IV variants as summarized in Table 1. Furthermore, molar ellipticity values of apoA-IV isoforms at 222 nm were measured as a function of guanidine chloride (GuHCl) at 25 °C to examine the chemical stability of apoA-IV isoforms *in vitro* (Fig. 1*D*). We identified that all three variants showed a biphasic denaturation plot in a dose–response manner with WT demonstrating the most pronounced biphasic denaturation curve. To compare the effect of chemical denaturation, we quantified EC_{50} values using a biphasic nonlinear regression model (Table 1). The initial transition signifies the disturbance of protein self-association in the solution, whereas the subsequent transition occurs at a greater concentration of GuHCl, indicating complete protein unfolding. As listed in Table 1, apoA-IV^{T347S} was quantified to have the lowest chemical and thermal denaturation points among the examined variants, and apoA-IV^{WT} showed the highest chemical and thermal denaturation points.

Fluorescence anisotropy showed molecular dynamics differences in apoA-IV

Molecular dynamics of C-terminal-labeled apoA-IV variants were measured *in vitro* utilizing fluorescence anisotropy. Specifically, the molecular tumbling of apoA-IV^{T347S} and apoA-IV^{Q360H} polymorphisms was compared with that of apoA-IV^{WT} in PBS at 37 °C (Fig. 1*E*). Our results showed statistically significant difference among these three common polymorphisms, with apoA-IV^{T347S} polymorphism demonstrating the lowest average normalized anisotropy values, while apoA-IV^{WT} exhibited the highest average normalized anisotropy value (Fig. 1*E*). The decreased fluorescence anisotropy observed with apoA-IV^{T347S} and apoA-IV^{Q360H} suggests that these two variants have a faster movement of the C-terminal domain compared with apoA-IV^{WT}.

Dimerized apoA-IV polymorphisms exhibited inhibition of platelet aggregation

The impact of dimerized apoA-IV on platelet function was examined to test whether dimerized apoA-IV protein isoforms (10), which exists in blood, can bridge adjacent platelets. Recombinant apoA-IV protein isoforms were chemically modified and linked using covalent spacers (10), and their effects on ADP-induced human platelet aggregation were investigated.

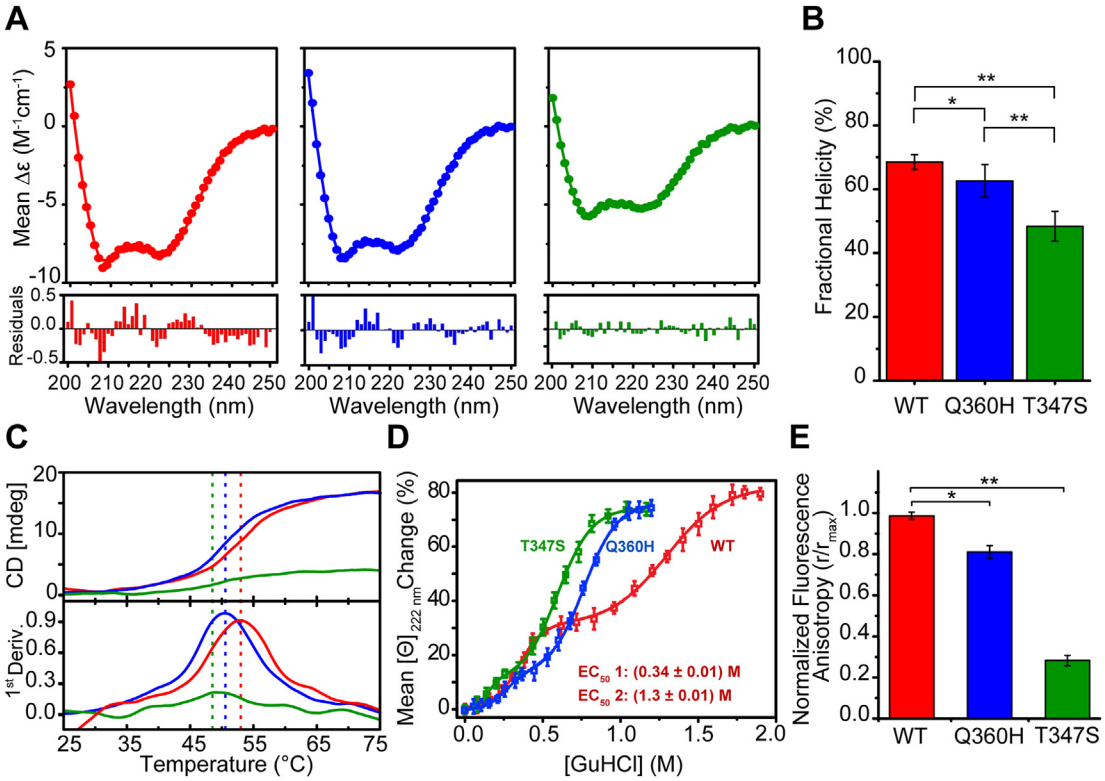

Figure 1. Protein folding and molecular tumbling analyses of apoA-IV polymorphisms. *A*, CD spectra for the average molar ellipticity *versus* wavelength of apoA-IV^{WT} (*red*), apoA-IV^{Q360H} (*blue*), and apoA-IV^{T347S} (*green*) in PBS at 37 °C. *B*, displays a comparison of percentage α-helix content (fractional helicity) of apoA-IV polymorphisms. *C*, shows the thermal stability analysis of apoA-IV proteins. *Dotted lines* signify T_m points of 53.2, 50.8, and 47.6 °C for apoA-IV^{WT} (*red*), apoA-IV^{Q360H} (*blue*), and apoA-IV^{T347S} (*green*), respectively. *D*, shows protein folding stability analysis of apoA-IV proteins in PBS at 25 °C as a function of guanidine chloride concentration. *E*, exhibits molecular tumbling examination using fluorescence anisotropy of fluorophore-labeled apoA-IV variants in PBS at 37 °C. Fluorescence anisotropy measures the rotational mobility of labeled C terminus with polarized light. Bar graph demonstrates that apoA-IV^{Q360H} tumbles faster than apoA-IV^{WT}, and apoA-IV^{T347S} tumbles faster than apoA-IV^{Q360H} and apoA-IV^{WT}. Mean normalized fluorescence anisotropy values are subtracted from an unconjugated fluorophore blank sample. Quantified values are listed in Table 1. *$p < 0.05$, **$p < 0.01$, N = 20. apoA-IV, apolipoprotein A-IV.

Our findings revealed that the dimerized apoA-IV protein isoforms exhibited a significantly greater inhibition of platelet aggregation compared with the unmodified heterogenic apoA-IV isoforms (Fig. 2, *A* and *B*). Upon analyzing the aggregation findings among dimer apoA-IV variants, we observed that the inhibitory effect was more pronounced in apoA-IV^{WT} dimer in comparison to the apoA-IV^{T347S} and apoA-IV^{Q360H} variants. This trend was also observed with the unmodified heterogenic apoA-IV isoforms (Fig. 2*B*). This is the first to show that dimerized apoA-IV, which contains two αIIbβ3-binding sites, is still inhibitory (but not bridging adjacent platelets) for platelet aggregation, demonstrating its important physiological role in cardiovascular and other platelet-related diseases.

Table 1
Quantified chemical and thermal denaturation data from CD spectroscopy

ApoA-IV variants	Chemical stability		Thermal stability
	First EC_{50} (M)	Second EC_{50} (M)	T_m (°C)
WT	0.34 ± 0.01	1.3 ± 0.01	53.2 ± 0.91
Q360H	0.26 ± 0.02	0.77 ± 0.01	50.8 ± 1.1
T347S	0.15 ± 0.02	0.60 ± 0.01	47.6 ± 1.0

EC_{50} values denote GuHCl concentration points at which unfolding occurred.
Data presented as mean ± 1 SD, N = 3.

Binding affinity and kinetics studies showed direct binding of apoA-IV to αIIbβ3

To investigate and compare the binding affinities of apoA-IV^{WT}, apoA-IV^{T347S}, and apoA-IV^{Q360H} polymorphisms with human platelet ligands and receptors, we developed immobilized apoA-IV biosensor probes utilizing an interferometry technique and characterized the kinetics parameters of apoA-IV with activated human platelets at 37 °C using an average weight of (1.6 ± 0.1) ng per activated platelets (38). We found that apoA-IV^{WT} demonstrated the strongest association constant (k_{on}), whereas apoA-IV^{T347S} variant yielded the weakest k_{on} among examined three variants (Fig. 3*A* and Table 2). We further tested binding kinetics of apoA-IV variants *versus* activated αIIbβ3, GPVI, Fg, fibronectin, individually and examined dissociation constant (K_d) values *in vitro* (Figs. 3*B* and S2). As presented in Table 2, our results showed that apoA-IV^{WT} exhibited the highest binding affinity with activated αIIbβ3, whereas the C-terminal mutations (apoA-IV^{T347S} and apoA-IV^{Q360H}) displayed weaker binding affinities compared with apoA-IV^{WT} (Fig. 3*B*). We found no detectable binding signal for apoA-IV interacting with either soluble Fg (Fig. S2*A*) and fibronectin (Fig. S2*B*) under the examined *in vitro* conditions. In reverse binding models, immobilized human serum albumin (HSA) and fibrinogen-like 1 protein

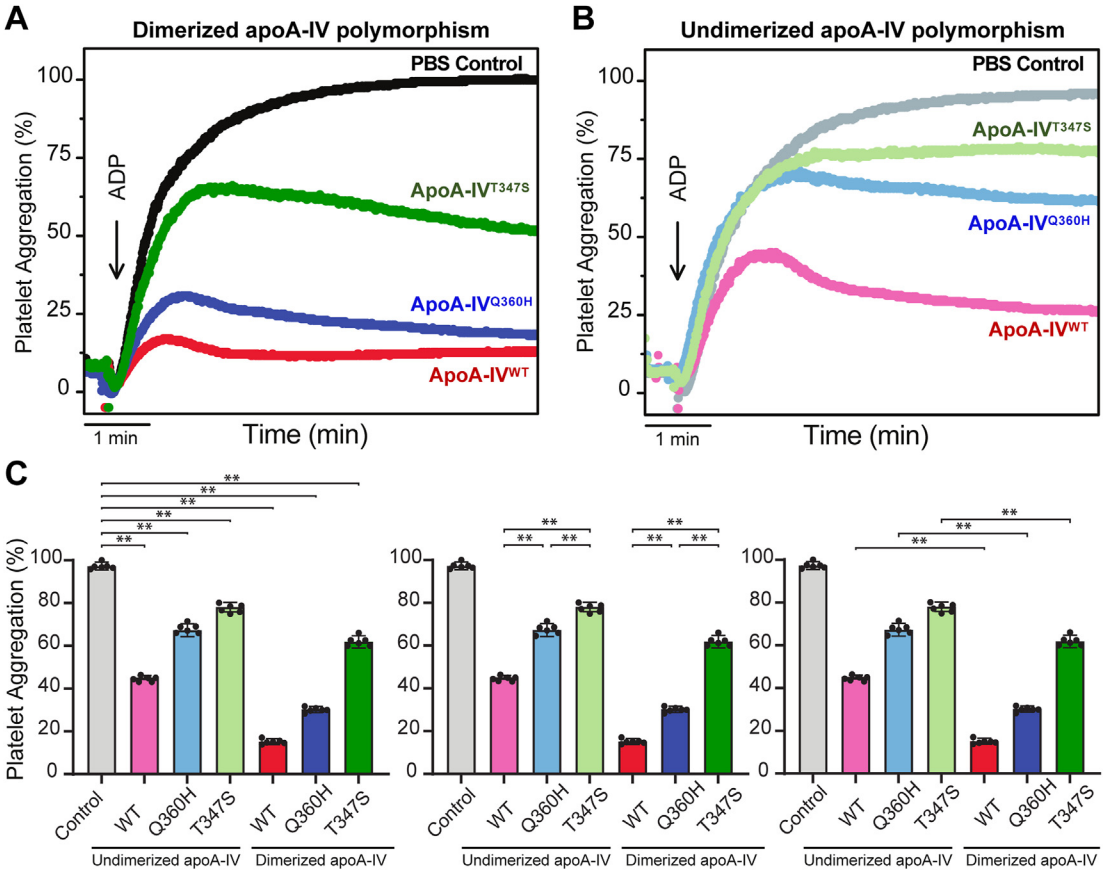

Figure 2. ApoA-IV polymorphisms inhibit human platelet aggregation. ADP-induced human platelet aggregation in platelet-rich plasma with and without the addition of 350 μg/ml (4 μM) apoA-IV^{WT} (*red*), apoA-IV^{Q360H} (*blue*), apoA-IV^{T347S} (*green*), and PBS control (*gray*) using light transmission aggregometry. *A*, presents superimposed tracings of platelet aggregation in the presence of dimerized apoA-IV (*dark colors*). *B*, shows overlaid tracings of platelet aggregation in the presence of undimerized homogenous apoA-IV (*light colors*). *C*, displays bar graphs for comparative statistical analyses of acquired platelet aggregation results. Each bar represents mean ± SD of maximum platelet aggregation. $^{**}p < 0.01$, N = 6. apoA-IV, apolipoprotein A-IV.

(FGL1) were tested against (2.0 ± 0.1) μM apoA-IV, and we did not detect binding signals within the experimental conditions. We examined the thermodynamics and dissociation parameters of apoA-IV^{WT}, apoA-IV^{Q360H}, and apoA-IV^{T347S} at 25 °C utilizing isothermal titration calorimetry (ITC) and quantified dimerization K_d values as presented in Table 3 (Fig. 4). The control ITC titrations conducted on Fg with apoA-IV variants did not yield any quantifiable heat of binding (Fig. S3).

Light scattering studies demonstrated multimeric conformation of apoA-IV

Dynamic laser light scattering and multiangle light scattering (MALS) techniques were utilized to study the self-association of apoA-IV polymorphisms *in vitro*. Our results showed a heterogenic mixture of apoA-IV multimers and quantified hydrodynamic radii (R_h) of 2.9, 2.7, and 3.4 nm for apoA-IV^{WT}, apoA-IV^{Q360H}, and apoA-IV^{T347S}, respectively, in PBS (Fig. 5*A*). Our size-exclusion chromatography (SEC)–MALS and nondenaturing PAGE analyses showed significant difference in dimerization properties of apoA-IV variants. We found that apoA-IV^{Q360H} eluted a larger amount of monomer conformation than dimer or trimer conformations (Fig. 5, *B* and *C*). We also found that both apoA-IV^{WT} and apoA-IV^{T347S} eluted larger amounts of dimer conformation than trimer or monomer. We found that apoA-IV^{T347S} polymorphism eluted the smallest amount of tetramer, or dimer of dimer, conformation among three apoA-IV isoforms (Fig. 5*C*).

Fluorescence quenching studies defined conformational change of apoA-IV

To study the structure unfolding mechanism of apoA-IV polymorphisms through lipid binding *in vitro*, we measured the intrinsic fluorescence emission of single tryptophan residue (W12) on the N termini of apoA-IV variants in titrations with 1,2-dimyristoyl-*sn*-glycero-3-phosphocholine (DMPC) at 37 °C. The intrinsic fluorescence emission of apoA-IV polymorphisms exhibited a dose-dependent rise with the addition of phospholipid DMPC (Fig. 6*A*). Analyzing the acquired fluorescence intensities and emission maxima, we found that apoA-IV^{T347S}, apoA-IV^{Q360H}, and apoA-IV^{WT} isoforms yielded a modest shift of (8 ± 3) nm in the emission spectra that were comparable in all three apoA-IV variants, suggesting conformational change in the folded structure of apoA-IV (Fig. 6, *B* and *C*). To further investigate this conformational change mechanism, we studied electron transfer properties of W12 in apoA-IV variants using the intrinsic fluorescence of

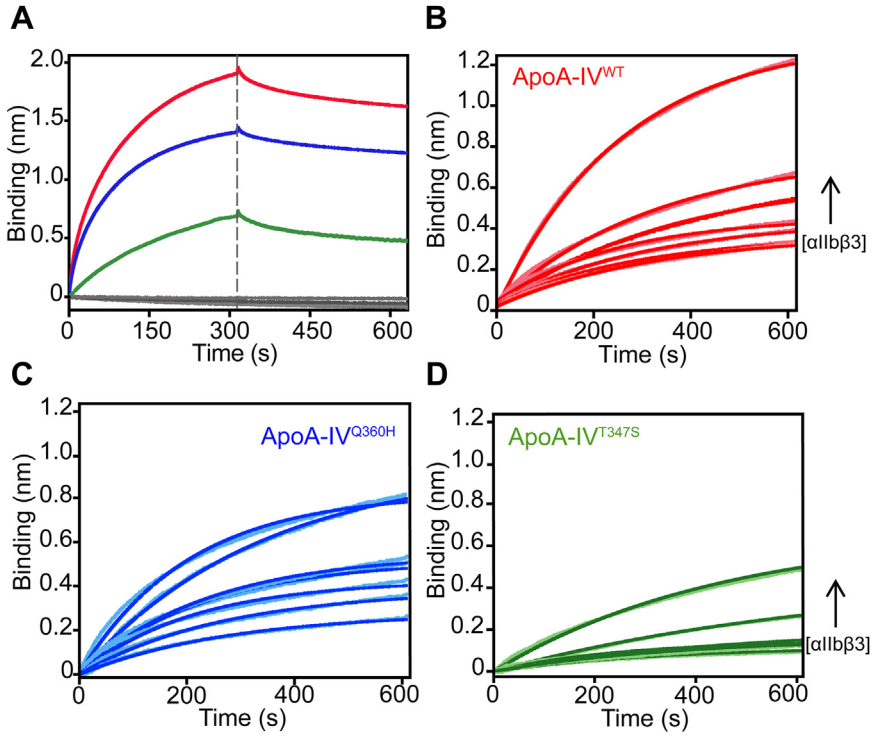

Figure 3. Direct binding affinity quantification of apoA-IV polymorphisms with purified human αIIbβ3. *A*, displays BLI sensograms for 0.2 μM apoA-IV polymorphisms as a function of activated human purified αIIbβ3 concentration in activation buffer at 1000 rpm, 37 °C (*B*) shows BLI kinetics sensograms for 0.2 μM apoA-IV^{WT}, (*C*) apoA-IV^{Q360H}, and (*D*) apoA-IV^{T347S} polymorphisms with solutions of gel-filtered platelets in an activation buffer (20 mM Tris, pH 7.4, 137 mM NaCl, 1 mM $CaCl_2$, 1 mM $MgCl_2$, 1 mM $MnCl_2$, 30% [v/v] glycerol) at 1000 rpm, 37 °C (N = 3). Quantified binding affinity values are listed in Table 2. apoA-IV, apolipoprotein A-IV; BLI, biolayer interferometry.

apoA-IV as a function of two different types of quenchers (sodium iodide and acrylamide) in the absence and presence of DMPC at 37 °C (Figs. 6*D*, and 7, *A*–*C*). To prevent the formation of triiodide ion, we added 1 μM sodium thiosulfate in sodium iodide solution and analyzed fluorescence titration isotherms as a function of each quencher concentration and quantified Stern–Volmer constants as summarized in Table 4.

FRET reveals spatial structure arrangement of apoA-IV

The spatial structure rearrangement and intramolecular distance of apoA-IV multimers in WT, T347S, and Q360H variants were measured utilizing two FRET techniques *in vitro* at 37 °C. We found that apoA-IV^{Q360H} and apoA-IV^{WT} isoforms emitted higher Förster efficiencies in buffer compared with that of apoA-IV^{T347S} (Fig. 7*D*), indicating close proximity of the C and N termini. We identified that the electron transfer efficiencies were increased immediately after DMPC was added and then decreased and remained steady as apoA-IV variants were mixed with DMPC at 37 °C and incubated for 30 min (Fig. 7*D*). We measured the intermolecular distance of each apoA-IV variant and found that the distance between C and N termini increases from (26 ± 4) Å in a homodimer conformation to (127 ± 14) Å with the addition of phospholipid DMPC, indicating that self-assembly structure of oligomeric apoA-IV was changed and rearranged, where C and N termini are farther apart from each other (Fig. 7*E*).

Table 2
Quantified direct binding affinity data for apoA-IV polymorphisms and human platelets and αIIbβ3 titrations using BLI

	Platelets	αIIbβ3
ApoA-IV variants	K_d (Platelets × 10^5 ml^{-1})	K_d (nM)
WT	1.5 ± 0.3	5.2 ± 0.2
Q360H	3.7 + 0.6	82 ± 3
T347S	4.8 + 0.8	397 ± 18

Data presented as mean ± 1 SD, N = 3.

Computational structure studies elucidate apoA-IV–αIIbβ3 binding interface

In silico computational structure modeling was used to analyze the effect of C-terminal mutations of apoA-IV on the structure alignment and binding interface residues with integrin αIIbβ3. While the overall topologies of apoA-IV variants were comparable, we found that C-terminal (S336–S376) helical domains of apoA-IV^{Q360H} and apoA-IV^{T347S} exhibited helix–turn conformations whereas apoA-IV^{WT} showed a continuous α-helix structure (Fig. 8, *A* and *B*). Measuring the distance between C-terminal domains from superimposed structures, we calculated that apoA-IV^{Q360H} and apoA-IV^{T347S} oriented 20 and 26 Å away from apoA-IV^{WT}, respectively (Fig. 9*A*). Analyzing the binding interfaces of apoA-IV with the available structure of the αIIbβ3 headpiece, we computed that 41 amino acids of apoA-IV^{WT}, including N-terminal D13, interacted with αIIbβ3 (Figs. 9*B* and 10*A*), while we found 33 and 27 residues for apoA-IV^{Q360H} and apoA-IV^{T347S}, respectively, we did not observe direct contribution of D13 in

Table 3
Dissociation of apoA-IV variants in PBS using ITC methods

ApoA-IV variants	K_{d1} (μM)	ΔH_1 (kcal mol^{-1})	$-T\Delta S_1$ (kcal mol^{-1})	K_{d2} (nM)	ΔH_2 (kcal mol^{-1})	$-T\Delta S_2$ (kcal mol^{-1})
WT	0.63 ± 0.13	2.7 ± 0.6	−11 ± 1	54 ± 17	−27 ± 3	21 ± 4
T347S	102 ± 51	−34 ± 1	−28 ± 1	—	—	—
Q360H	No heat detected					

Data presented as mean ± 1 SD, N = 3.

apoA-IV^{Q360H} and apoA-IV^{T347S} binding αIIbβ3 (Fig. 10, *A* and *B*), indicating apoA-IV variants exhibited distinct binding sites on αIIbβ3 headpiece.

Discussion

The impact on the structural stability and functional properties of the three most prevalent apoA-IV protein isoforms were examined utilizing a series of structural and functional assays. Binding kinetics characterizations showed that mutations in the C-terminal region of apoA-IV, specifically apoA-IV^{T347S} and apoA-IV^{Q360H} polymorphisms, can affect the structure of apoA-IV and alter the binding properties of apoA-IV to platelet integrin αIIbβ3. These findings explain our previous observations, wherein N-terminal mutations of D5/D13 abridged the inhibitory effects of apoA-IV^{WT} on platelet aggregation (4, 5). In this study, we show that apoA-IV^{WT} and apoA-IV^{Q360H} exhibit higher fractional helicity than that of apoA-IV^{T347S} (Fig. 1*A*). The thermal and chemical stability characterizations demonstrate a significant T_m decrease with apoA-IV^{T347S} and apoA-IV^{Q360H} polymorphisms compared with that of apoA-IV^{WT} (Fig. 1 and Table 1). These results agree with previous studies, where helix-promoting modifications of apoA-IV favored the higher oligomeric topology and subsequently higher rates of phospholipid binding (37, 39, 40). The α-helix bundle motif is a key property for lipid-binding protein stability and amphipathic functionality in aqueous environments such as plasma. When apolipoproteins bind to lipids, they form a protective bundle that can be enthalpically favorable to compensate for the unfavorable entropy (41). The apoA-IV^{T347S} variant displays reduced T_m values in contrast with apoA-IV^{WT} and apoA-IV^{Q360H}, indicating a less stable protein structure. Thus, apoA-IV^{T347S} is more likely to interact with the charged and hydrophobic phospholipids present in the bloodstream (42).

The fluorescence anisotropy analysis of apoA-IV variants demonstrates significant differences among the three polymorphisms. The molecular tumbling, the rotational movement of molecules around their center of gravity in three spatial axes, and fluorescence polarization and anisotropy values are inversely correlated (43). High fluorescence anisotropy values observed for apoA-IV^{WT} signifies slower C-terminal tumbling to that observed with apoA-IV^{Q360H} and apoA-IV^{T347S} polymorphisms. The order of tumbling observed with the examined apoA-IV proteins examined agrees with the order of stability yielded from the chemical and thermal denaturation assays (Fig. 1, *B*–*F*).

We also studied the impact of apoA-IV on platelet function and tested if dimerized apoA-IV, which physiologically exists in blood, can crosslink platelets. Consistent with our earlier

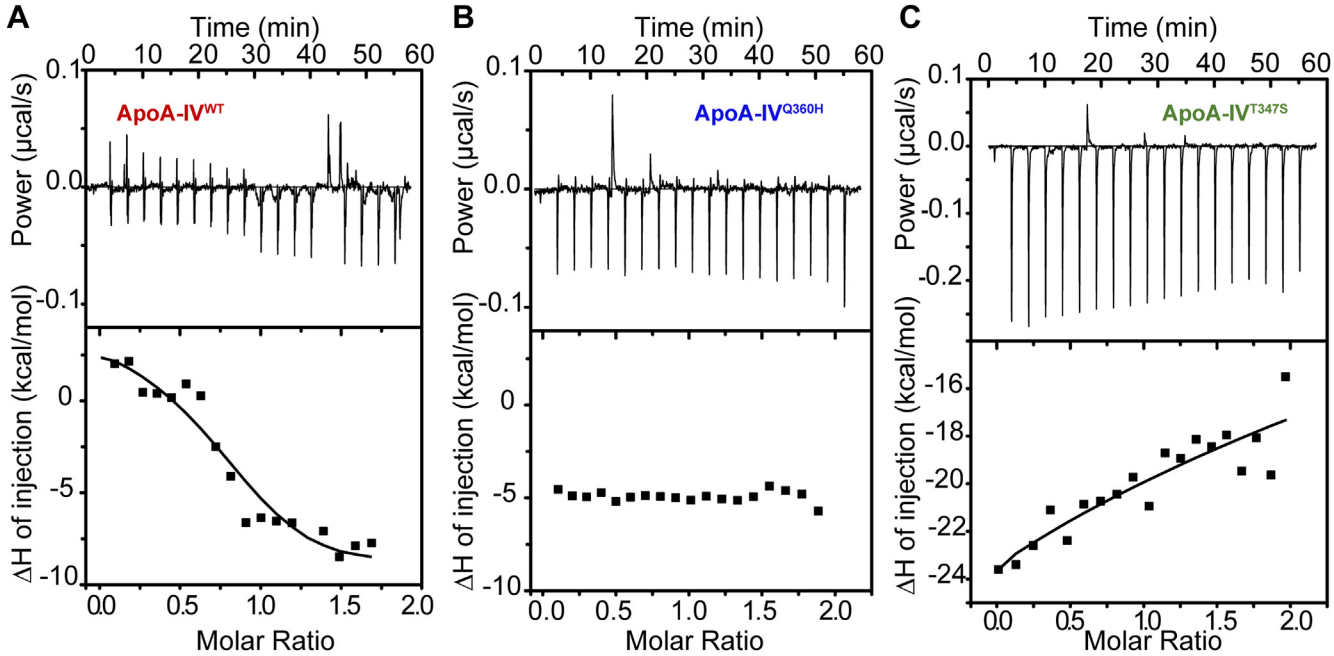

Figure 4. Isothermal titration calorimetry thermograms of apoA-IV polymorphisms. Comparative analysis of multimer dissociation parameters of (*A*) apoA-IV^{WT}, (*B*) apoA-IV^{Q360H}, and (*C*) apoA-IV^{T347S} in PBS (N = 3). apoA-IV, apolipoprotein A-IV.

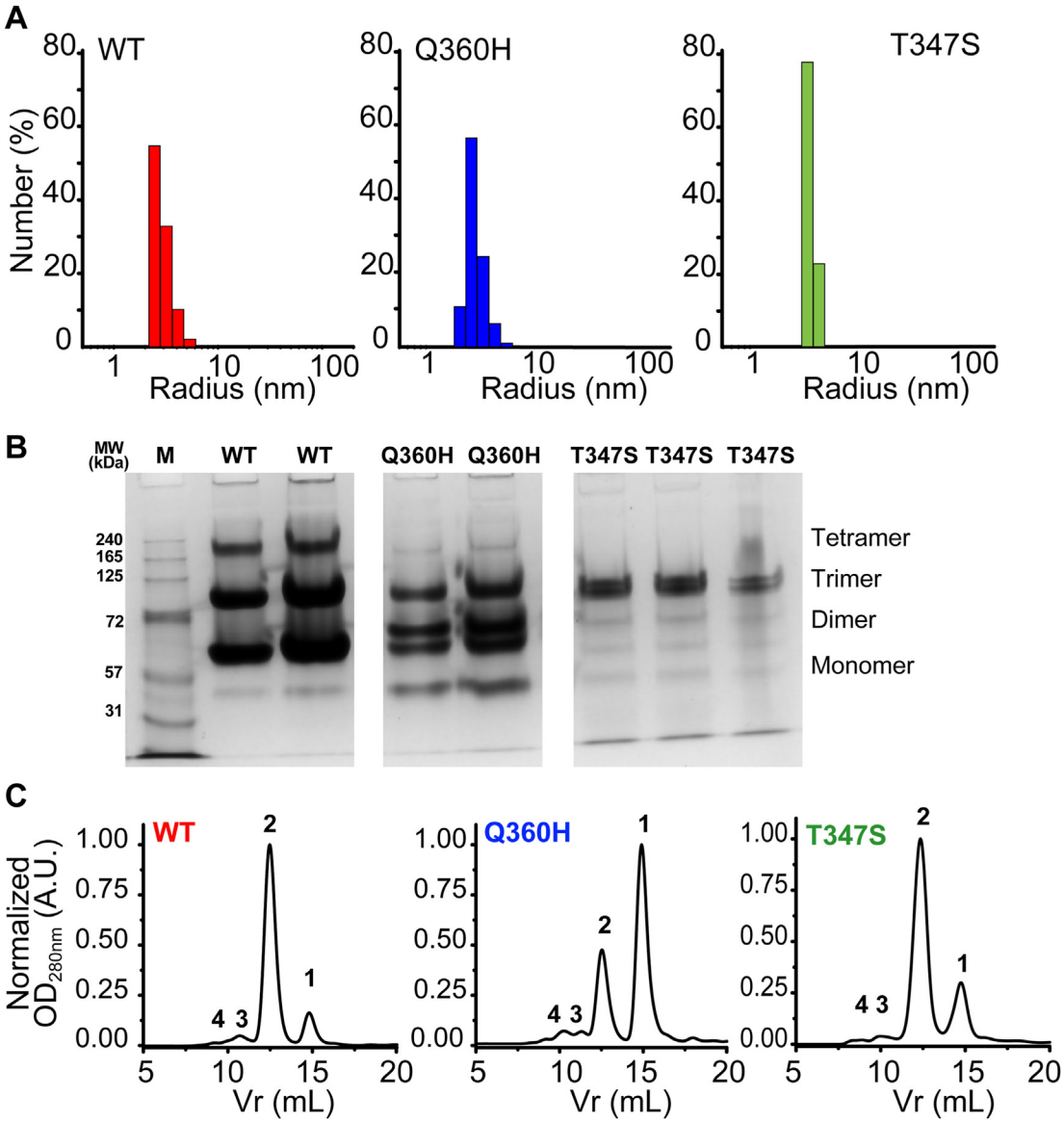

Figure 5. Characterization of molecular size and multimer formation of studied apoA-IV polymorphism. *A*, shows molecular size analysis of apoA-IV^{WT} (*red*), apoA-IV^{Q360H} (*blue*), and apoA-IV^{T347S} (*green*) using dynamic laser light scattering. *B*, demonstrates variations in multimer formation properties of apoA-IV on 8% PAGE under nondenaturing (pH 7.4) conditions at 25 °C. M denotes protein molecular weight marker. Electrophoresis was performed on the displayed lanes within a single gel, and the spacer lanes were removed to enhance clarity. *C*, shows multiangle light scattering demonstrated multimer diffusion properties of apoA-IV variants in PBS (pH 7.4) at 25 °C. Numeric annotations 1 to 4 represent eluates corresponding to monomer, dimer, trimer, and tetramer, respectively, N = 4. apoA-IV, apolipoprotein A-IV.

studies and other reports (4, 5, 44, 45), we show that chemically dimerized apoA-IV^{WT} inhibited platelet aggregation significantly more than dimerized apoA-IV^{Q360H} and dimerized apoA-IV^{T347S}. Our results suggest that dimerized apoA-IV polymorphisms do not crosslink platelets and maintain thrombosis-attenuating effect as previously described (4, 5). The dimerization may be similar to plasma fibronectin (dimerized with the same polypeptide), in which the two RGD-αIIbβ3 binding sites are close to each other and insufficient to bridge the adjacent platelets but rather may enhance its inhibitory effect *via* enhancing the local avidity to block platelet αIIbβ3 integrin (34, 46). To the best of our knowledge, this study is the first to present evidence suggesting that dimerized apoA-IV in the blood does not promote, but inhibits, platelet aggregation, and the polymorphisms attenuates this process.

In addition, immobilized apoA-IV biosensor probes were developed to investigate and characterize the kinetics parameters of apoA-IV variants with activated human platelets. The apoA-IV^{WT} variant shows the strongest binding affinity, whereas apoA-IV^{T347S} variant had the weakest binding affinity (Table 2). These results agree with our platelet aggregation results. The binding kinetics of apoA-IV variants with activated αIIbβ3 were tested. The observed binding affinity for apoA-IV^{WT} agrees with our previous published data (4, 5, 47). The direct binding affinity of apoA-IV with GPVI, platelet receptor for collagen and fibrin(ogen) interactions (48), was examined as a control and demonstrated no significant binding

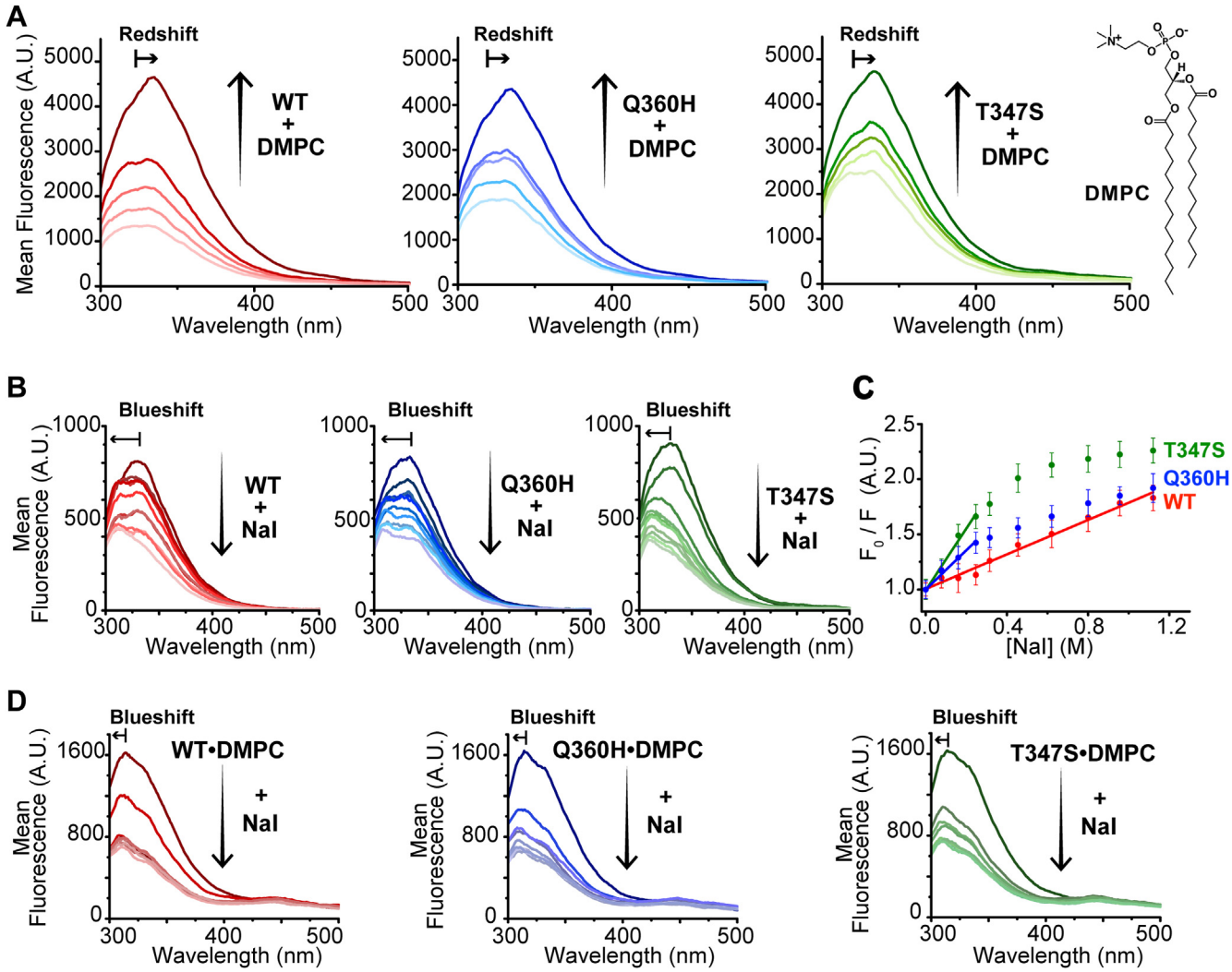

Figure 6. Intrinsic fluorescence enhancement and quenching titrations demonstrating the conformational changes of examined apoA-IV polymorphisms. *A*, shows fluorescence emission increase and redshifted spectra of apoA-IV^{WT} (*red*), apoA-IV^{Q360H} (*blue*), and apoA-IV^{T347S} (*green*) as a function of titrations with phospholipid (DMPC). *B*, exhibits fluorescence emission quenching and blueshifted spectra of apoA-IV polymorphisms unbound to DMPC as a function of sodium iodide concentration. *C*, shows overlaid Stern–Volmer plots for fluorescence quenching analysis. *D*, displays fluorescence emission quenching and blueshifted spectra of apoA-IV polymorphisms bound to DMPC as a function of sodium iodide concentration. Data acquired in 20 mM Hepes, pH 7.4, 140 mM NaCl at 37 °C. apoA-IV, apolipoprotein A-IV; DMPC, 1,2-dimyristoyl-*sn*-glycero-3-phosphocholine.

signals. The absence of binding affinities for apoA-IV variants with soluble Fg, fibronectin, and GPVI signifies the binding specificity and hence the importance of apoA-IV and αIIbβ3 interactions. Our findings agree with previous studies on the main atherogenic constituent of lipid-binding proteins that substantiated the binding properties of lipoprotein(a) with plasma Fg and fibronectin (49, 50). It is well documented that the process of blood coagulation occurs on the surface of phospholipids circulating in plasma (51–53). Existing literature indicates that phospholipids support plasma fibrin polymerization *via* adsorption of Fg onto phospholipid surfaces (54), thus, we think apoA-IV may regulate fibrinolysis by solubilizing plasma phospholipids. The negatively charged phospholipid bilayers provide a binding platform, where coagulation factors interact and transform proenzyme into active enzymes (30, 31, 55, 56).

We quantified the multimeric diffusion properties of apoA-IV variants and show that apoA-IV^{T347S} variant yields the lowest fraction of tetramer conformation among the apoA-IV variants tested. We attribute this to the increased hydrophobic shielding and negative charge density to the C terminus of apoA-IV^{Q360H} that can interfere with the domain-swapping dimerization process (10, 40, 57). A large fraction of monomeric apoA-IV^{Q360H} distribution can also explain weak platelet binding and small inhibition of platelet aggregation than what we observed with apoA-IV^{WT}. We performed the structure alignment of apoA-IV^{Q360H} and apoA-IV^{T347S} variants individually with apoA-IV^{WT} and identified that C-terminal α-helix structure of apoA-IV^{Q360H} had a bent conformation, where it folded closer to the core helical bundle whereas C-terminal α-helix structure of apoA-IV^{T347S} was found to be oriented away from the core helical bundle (Fig. 10). These findings agree with our fluorescence anisotropy analyses, where we detected higher molecular tumbling for apoA-IV^{T347S} and apoA-IV^{Q360H} variants than for apoA-IV^{WT}. By comparing the predicted structures of apoA-IV

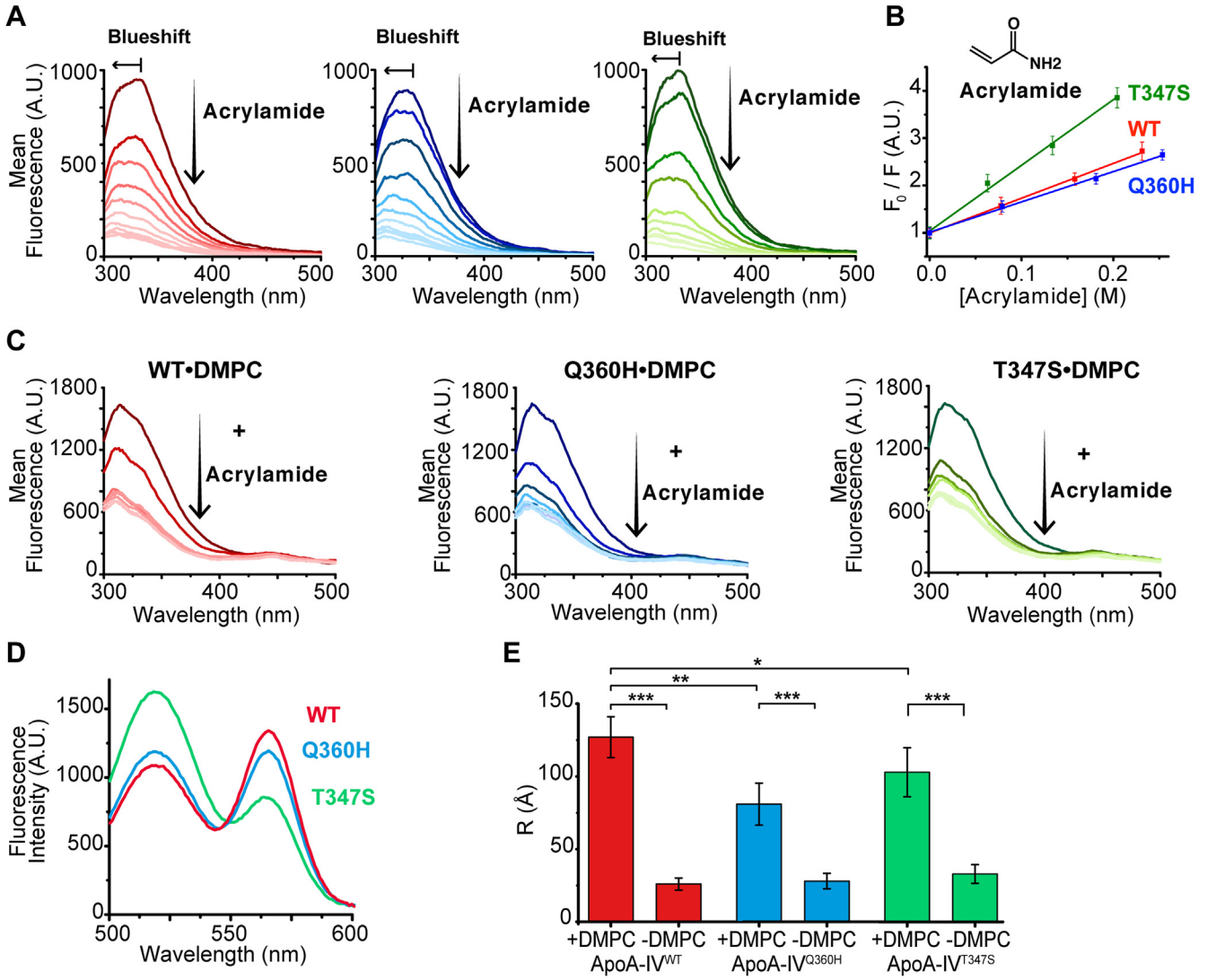

Figure 7. Intrinsic fluorescence titrations reveal conformational changes linked to apoA-IV polymorphisms. *A*, shows fluorescence emission quenching and blueshifted spectra of apoA-IV polymorphisms unbound to phospholipid (DMPC) as a function of acrylamide concentration. *B*, displays overlaid Stern–Volmer plots for fluorescence quenching analysis. *C*, exhibits fluorescence emission quenching of apoA-IV polymorphisms bound to DMPC as a function of acrylamide concentration. *D*, fluorescence emission spectra for FRET analysis of apoA-IV polymorphisms. Data acquired in 20 mM Hepes, pH 7.4, 140 mM NaCl at 37 °C. *E*, intermolecular distance comparison of apoA-IV polymorphisms from FRET data without and with threefold molar ratio of DMPC. *$p < 0.05$, **$p < 0.01$, ***$p < 0.001$, N = 3. apoA-IV, apolipoprotein A-IV; DMPC, 1,2-dimyristoyl-*sn*-glycero-3-phosphocholine.

polymorphisms, we were able to identify significant disruptions in the binding interfaces of apoA-IV^{T347S} and apoA-IV^{Q360H} variants with αIIbβ3 compared with that in apoA-IV^{WT}–αIIbβ3 binding interface. Our results demonstrate that D5 and D13 residues in apoA-IV have key roles. The D5 residue folds inward and interacts with R326 from the core helix, stabilizing the core bundle and exposing the binding interface. D13 and other 40 residues of apoA-IV^{WT} form a direct interaction platform and shield GRGDSP binding site of Fg and αIIbβ3. ApoA-IV^{Q360H} mutation yields in a binding interface that is reduced to 33 residues, whereas apoA-IV^{T347S} mutation results in a binding interface that is reduced to 27 residues. Neither apoA-IV^{Q360H} nor apoA-IV^{T347S} binding interface contained D5/D13 residues. The decrease in binding interface residues obtained through our computational analysis is supported by our experimental binding affinity results. We previously showed that the removal of the N terminus (Δ1–38) from recombinant apoA-IV eliminated its ability to inhibit platelet activity, whereas the deletion of the C terminus (Δ336–376) actually increased this inhibitory effect (4). These findings suggested to us that we further explore the molecular tumbling associated with apoA-IV polymorphisms. Our results

Table 4
Stern–Volmer constants (K_{SV}) of apoA-IV polymorphisms quantified from intrinsic fluorescence quenching titrations

	Acrylamide (M^{-1})	Sodium iodide (M^{-1})
ApoA-IV variants	-DMPC	-DMPC
WT	7.3 ± 0.1	0.78 ± 0.09
Q360H	6.4 ± 0.2	1.8 ± 0.1
T347S	13.9 ± 0.7	2.8 ± 0.3

Data presented as mean ± 1 SD, N = 3.

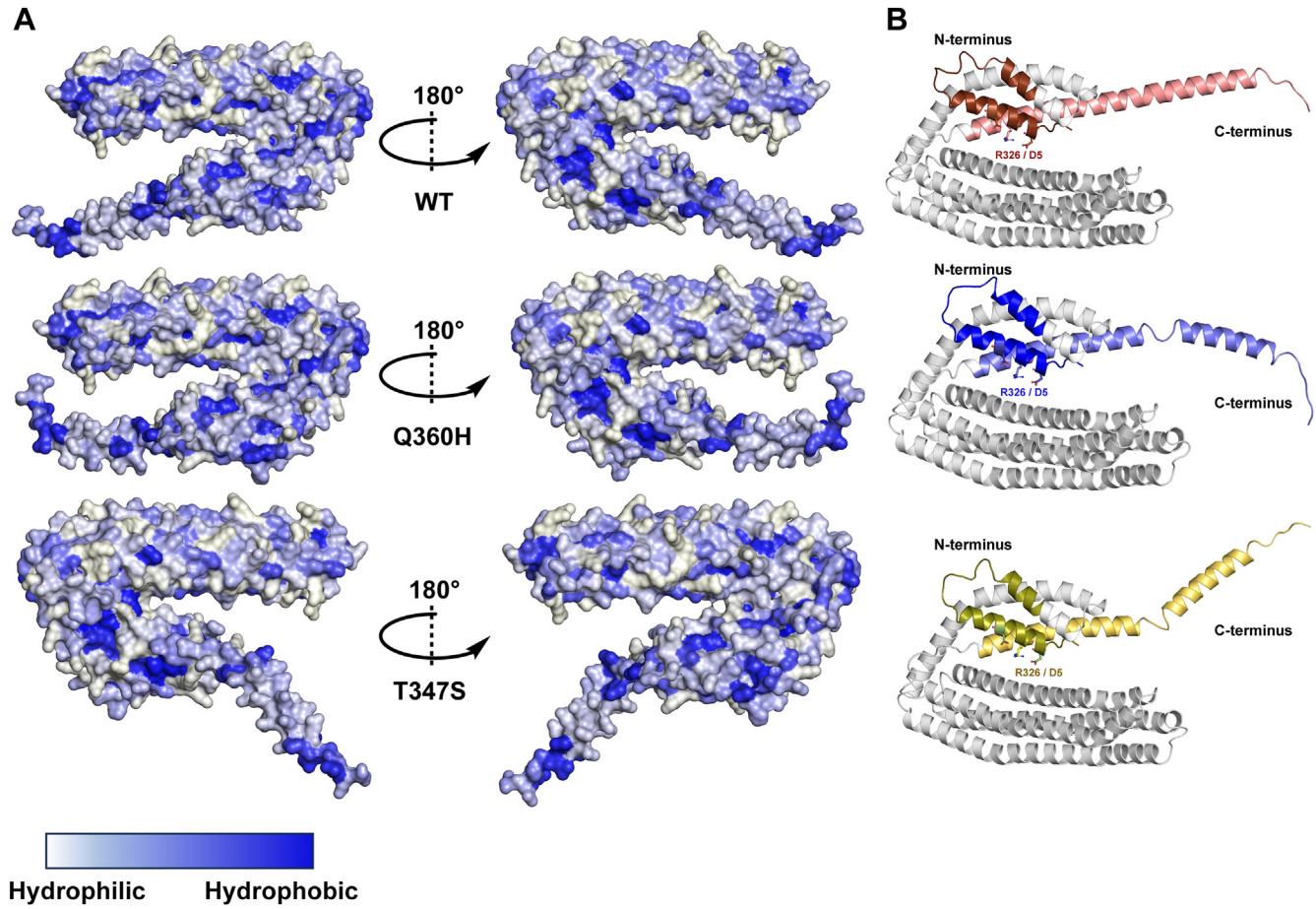

Figure 8. Comparison of overall *in silico* computational structure elucidation of studied apoA-IV polymorphisms in their monomeric conformations. *A*, demonstrates amphipathic nature of apoA-IV^{WT}, apoA-IV^{Q360H}, and apoA-IV^{T347S} *white color* denotes hydrophilic surfaces, and *blue shades* signify hydrophilic regions. *B*, shows differences in spatial orientations of N and C termini of apoA-IV^{WT} (*red*), apoA-IV^{Q360H} (*blue*), and apoA-IV^{T347S} (*olive*). Proximity and side-chain interaction of aspartic acid (D5) and arginine (R326) residues are denoted on each structure. apoA-IV, apolipoprotein A-IV.

demonstrate that the steric hindrance resulting from the tumbling of a loosely folded C terminus of apoA-IV may disrupt the interaction between two apoA-IV molecules and their binding sites, thereby explaining the enhanced inhibitory function observed upon C-terminal deletion.

To conclude, we demonstrate significant fractional helicity and structural stability reduction in apoA-IV^{T347S} compared with apoA-IV^{WT} and apoA-IV^{Q360H} isoforms. Our molecular dynamics analysis indicates that the C terminus of apoA-IV^{Q360H} tumbles slightly faster than apoA-IV^{WT}, and apoA-IV^{T347S} tumbles the fastest among examined three variants. The observed trend supports our platelet aggregation, binding affinity, and kinetics results for apoA-IV and αIIbβ3 utilizing our light transmission aggregometry and biolayer interferometry (BLI) assays. We further elucidate apoA-IV–αIIbβ3 binding interface and demonstrate a biomolecular mechanism for variable functions observed in the most common human apoA-IV polymorphisms: apoA-IV^{WT}, apoA-IV^{Q360H}, and apoA-IV^{T347S}. Our structural analyses provide valuable insights into the structural effects of C-terminal mutations and their potential impact on the function of apoA-IV, which is important for platelets, lipid metabolism, and blood coagulation including fibrinolysis. Notably, as platelets are versatile cells, our data should have broad impact in platelet-related diseases, such as inflammation and immune response, particularly the chronic process of atherosclerosis.

Experimental procedures

Materials

All chemicals and reagents were obtained from Sigma–Aldrich and used as received unless otherwise stated. Buffer solutions were prepared in distilled deionized water with a measured resistivity ≥18.2 MΩ cm (Milli-Q) at 25 °C and filtered using 0.45 μm filters and sterilized using 0.11 to 0.22 μm filters. Purified human platelet integrin αIIbβ3 (Innovative Research), purified human plasma Fg, and purified human plasma fibronectin were used as received without any modifications. The protein concentrations were measured using ultraviolet light absorbance at 205, 214, and 280 nm using computed molar extinction coefficient values (Table S1) as described (58). All procedures using human blood samples were approved by the Research Ethics Board of St Michael's Hospital, Toronto, Canada.

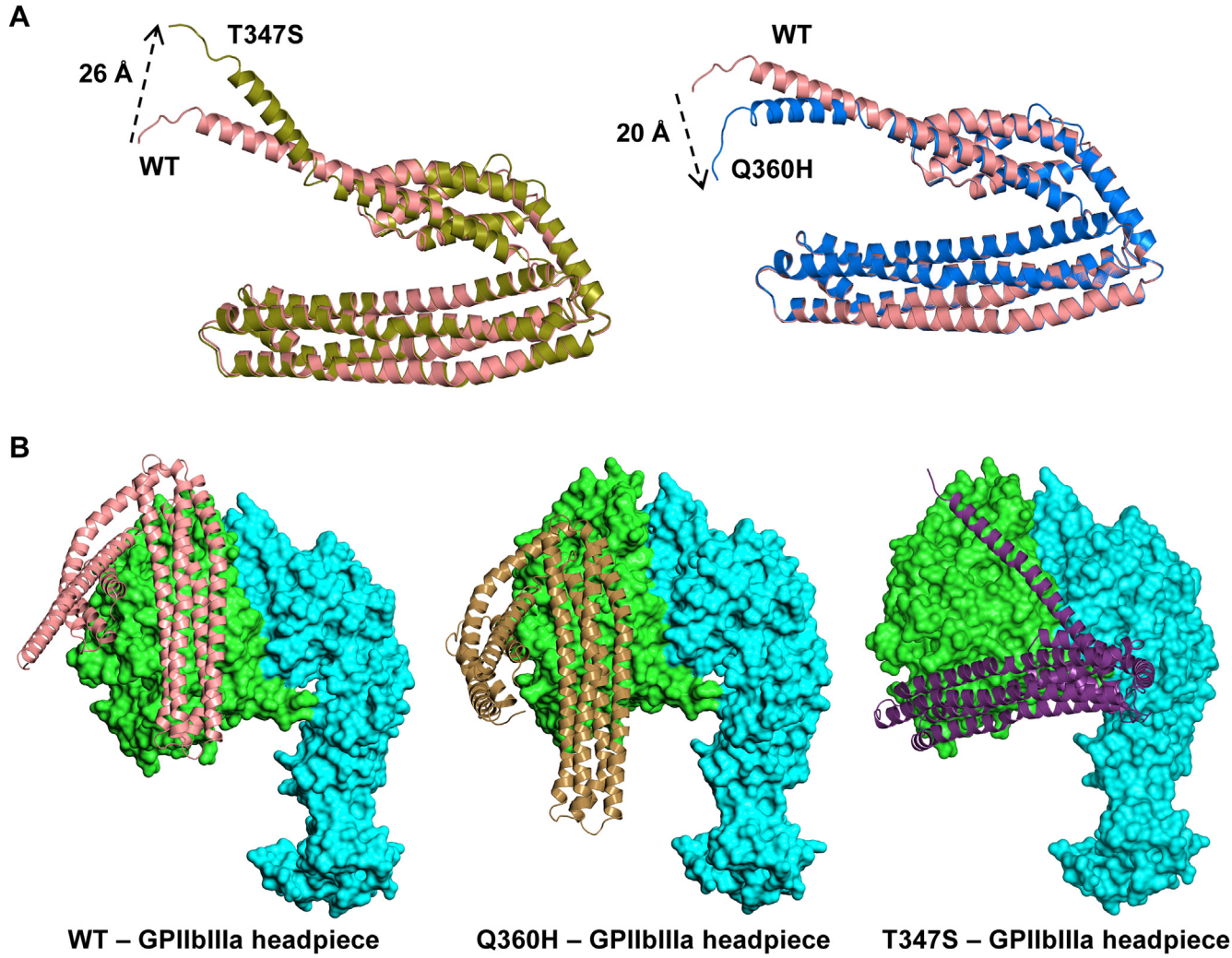

Figure 9. Comparison of C-terminal conformations of examined apoA-IV polymorphisms. *A*, demonstrates superimposed comparison of apoA-IV^{WT} (*red*) with apoA-IV^{T347S} (*olive*) on the *left* and superimposed comparison of apoA-IV^{WT} (*red*) with apoA-IV^{Q360H} (*blue*) on the *right*. Distance variations in the spatial orientations are denoted on superimposed structures. *B*, shows differences in spatial orientations and interactions of apoA-IV^{WT} (*light red*), apoA-IV^{Q360H} (*gold*), and apoA-IV^{T347S} (*purple*) with the headpiece structure of GPIIbIIIa (αIIbβ3). Protein surface representation of GPIIbIIIa (Protein Data Bank code: 3ZE2) are shown in *green* and *blue*, respectively. apoA-IV, apolipoprotein A-IV.

Protein expression and purification

Recombinant human apoA-IV^{WT}, apoA-IV^{Q360H}, and apoA-IV^{T347S} proteins were individually expressed in *Escherichia coli* BL21 (DE3). Full-length human apoA-IV variants were subcloned into the pET30a *E. coli* expression plasmid containing C-terminal 6× His tag and tobacco etch virus protease cleavage. The proteins were expressed by 1 mM isopropyl-β-D-1-thiogalactopyranoside induction (4, 8). Harvested cell pellets were lysed using an ultrasonic processor (Sonics) and purified using SuperFlow nickel–nitrilotriacetic acid (Ni–NTA; Invitrogen) columns followed by overnight dialysis in 20 mM Tris buffer, pH 7.4, 137 mM NaCl for binding analyses and separately in PBS (10 mM sodium phosphate buffer, pH 7.4, 137 mM NaCl, and 2.7 mM KCl) using (13 ± 1) kDa molecular weight cutoff membranes (Thermo Fisher) at 4 °C. The purification tag was then cleaved using the tobacco etch virus protease overnight at 4 °C and stopped with 0.1 mM phenylmethylsulfonyl fluoride for 2 h. The cleaved tag was removed using the Ni–NTA columns, collecting the eluent purified protein. Purity of proteins was assessed with SDS-PAGE analysis and One-Step Blue (Biotium) staining method. Electrophoretic mobility shift assays were performed utilizing a nondenaturing PAGE technique at 25 °C as previously described (44, 59, 60).

Size-exclusion chromatography

The SEC experiments were carried out on an ÄKTA Pure FPLC system utilizing a Superdex 200 Increase 10/300 column (GE Healthcare). The column was equilibrated with two column volumes of PBS running buffer (pH 7.4) containing 1 mM EDTA prior to each experiment unless otherwise stated. To evaluate oligomeric redistribution of apoA-IV variants, the physiological midrange concentration (200 μg/ml) of purified recombinant apoA-IV proteins was incubated at 37 °C in running buffer. At different time intervals, 100 μl of each apoA-IV variant was injected onto the

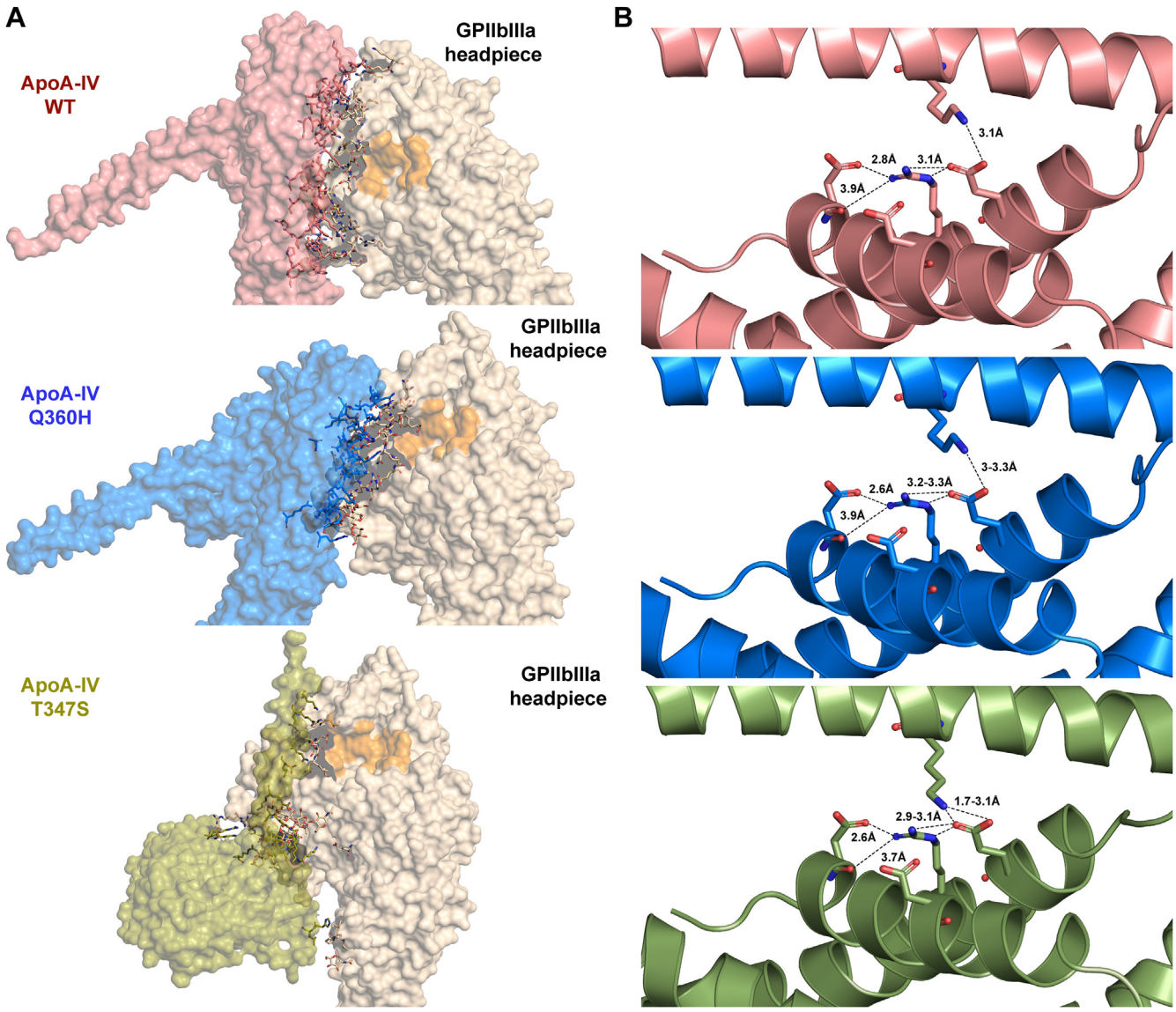

Figure 10. Structural elucidation of direct interactions of studied apoA-IV polymorphisms. *A*, demonstrates differences in the RGD motif region (*orange*) on GPIIbIIIa headpiece domain (Protein Data Bank code: 3ZE2, *gold*) covered by the binding sites of apoA-IV^{WT} (*red*), apoA-IV^{Q360H} (*blue*), and apoA-IV^{T347S} (*olive*). *B*, shows zoomed in *ribbon representations* for intermolecular helix–helix interactions of folded apoA-IV^{WT} (*red*), apoA-IV^{Q360H} (*blue*), and apoA-IV^{T347S} (*olive*) structures. apoA-IV, apolipoprotein A-IV.

column and experiments were run at a constant rate of 0.5 ml/min. The elution process was monitored by measuring the absorbance of eluate at 280 nm. Experiments were recorded and analyzed using the provided Unicorn software package (37, 61). The molecular size of the apoA-IV polymorphic multimers was assessed utilizing MALS with an Infinity-II HPLC (Agilent) and miniDAWN TREOS and OptiLab T-rEX refractive index detectors (Wyatt). The system was equilibrated in the sample buffer for 18 h before the first injection and calibrated using 2 mg/ml bovine serum albumin standard. Purified recombinant apoA-IV samples (50–100 µl) were injected on to the column and run at a constant rate of 0.5 ml/min. ASTRA software (Wyatt) was used to analyze the chromatograms and determine molecular masses (62).

Chemical modification of proteins

Recombinant human apoA-IV^{WT}, apoA-IV^{Q360H}, and apoA-IV^{T347S} proteins with a C-terminal cysteine tag were generated in the same manner as described previously and conjugated with Alexa Fluor 488, or fluorescein isothiocyanate (FITC) (Thermo Fisher) *via* a thiol-maleimide reaction. N-terminal apoA-IV samples were conjugated with Alexa Fluor 555 (Thermo Fisher) *via* *N*-hydroxysuccinimide ester reactions in 20 mM Hepes buffer, pH 7.4, 137 mM NaCl at 4 °C as described (63–65). Unconjugated cysteine residues were blocked with twofold concentration of *N*-ethylmaleimide. In separate experiments, 20 µM apoA-IV variants were cross-linked using 0.2 mM *bis*-sulfosuccinimidyl for 20 h at 4 °C, quenched with 1 M Tris buffer pH 7.4, and buffer-exchanged in 20 mM Hepes, pH 8.1, and 140 mM NaCl (10, 66).

Dimerized apoA-IV proteins were purified using SEC as described previously.

Platelet preparation and aggregation assays

Human blood samples were drawn from antecubital veins of healthy volunteers after providing informed consent. Human platelet-rich plasma and platelet-poor plasma were obtained by centrifugation at 250*g* for 8 min and a double spin at 5000*g* for 10 min, respectively, at 25 °C. Gel-filtered platelets were purified from platelet-rich plasma using a Sepharose 2B chromatography column with 5 mM 1,4-piperazinediethanesulfonic acid buffer, pH 7.0, 137 mM NaCl, 4 mM KCl, and 5.55 mM glucose as we previously described. To maintain the molar concentration of apoA-IV in agreement with our previously published data (4), a concentration of 350 μg/ml (4 μM) chemically dimerized as well as undimerized apoA-IV variants was used. After an incubation of 5 min, with testing samples or blank PBS (10 mM sodium phosphate, pH 7.4, 137 mM NaCl, and 2.7 mM KCl) at 37 °C. Platelet aggregation was initiated by addition of 5 μM ADP agonist, stirred at 1000 rpm, and monitored *in vitro* for a minimum of 8 min using a light transmission aggregometer (Chrono-Log) as we previously described (4, 67).

BLI assays

Recombinant His-tagged human apoA-IV^{WT}, apoA-IV^{Q360H}, and apoA-IV^{T347S} protein isoforms (0.2 μM) were separately immobilized onto hydrated Ni–NTA biosensor probes using an Octet RH16 interferometer (Sartorius) and tilted-bottom microplates. The probes were quenched in SuperBlock (Thermo Fisher) and equilibrated in binding buffer (20 mM Tris, pH 7.4, 137 mM NaCl, and 30% [v/v] glycerol) containing αIIbβ3 activation divalent salts (1 mM $MgCl_2$, 1 mM $CaCl_2$, and 1 mM $MnCl_2$) at 37 °C, 1000 rpm. The association (k_{on}) and dissociation (k_{off}) rates were measured to quantify the affinity parameters of apoA-IV variants with αIIbβ3, GPVI-Fc, Fg, and fibronectin. The effect of the binding buffer on the threshold of detection was optimized, and raw data were subtracted from the corresponding blank buffer samples. His-tagged recombinant HSA (Abcam) and His-tagged recombinant FGL1 (Innovative Research) were used as controls in a reverse binding model. HSA and Fg were immobilized onto separate control probes, and binding signals were monitored with His tag–free apoA-IV^{WT}, apoA-IV^{Q360H}, and apoA-IV^{T347S} proteins in solution as described previously. The acquired data were fit to a global binding model and analyzed to quantify the dissociation constant (K_d) using the supplied Octet software package as we previously described (47, 68, 69).

Platelet binding kinetics assays

Employing immobilized recombinant apoA-IV^{WT}, apoA-IV^{Q360H}, and apoA-IV^{T347S} biosensors and the described BLI method, the binding kinetics parameters (k_{on} and k_{off}) *versus* activated human gel–filtered platelets were measured in binding buffer (20 mM Tris, pH 7.4, 137 mM NaCl, 30% [v/v] glycerol) containing activation divalent salts (1 mM $MgCl_2$, 1 mM $CaCl_2$, and 1 mM $MnCl_2$) at 37 °C, 1000 rpm. Gel-filtered platelets were fixed by mixing platelets in a solution of 2% (v/v) paraformaldehyde at 37 °C for 10 min and washed three times between each step (5, 47).

ApoA-IV kinetics assays

The rate of lipid binding was determined using separate mixtures of apoA-IV^{WT}, apoA-IV^{Q360H}, apoA-IV^{T347S} proteins, and DMPC as a function of time at 37 °C. ApoA-IV protein solutions (0.2 mg/ml) were added to threefold concentration of DMPC suspensions in 20 mM Hepes buffer, pH 7.4, and 140 mM NaCl. Utilizing 96-well transparent plates (Thermo Fisher) and a Synergy Neo2 (BioTek) microplate reader, the absorbance values at 280 nm were monitored for 30 min (37, 70). The acquired data from triplicated experiments were averaged and normalized to the initial absorbance values and analyzed using the first-order decay model as we described (47, 63).

CD spectroscopy

The secondary structures of (2.5 ± 0.5) μM of purified recombinant human apoA-IV^{WT}, apoA-IV^{Q360H}, and apoA-IV^{T347S} proteins were determined by acquiring CD spectra, immediately after SEC elution, utilizing a Jasco J-1500 spectropolarimeter and 1-mm path length quartz cuvettes in a wavelength range from 195 to 250 nm at 1 nm/s acquisition rate. The temperature was kept constant at 37 °C using a Peltier controller (71). The α-helix content (fractional helicity) was calculated from the delta epsilon (M^{-1} cm^{-1}) values that were deconvoluted from acquired CD spectra in a wavelength range of 200 to 250 nm using BESTSEL software package (58, 72, 73).

Fluorescence anisotropy assays

The molecular tumbling of apoA-IV^{WT}, apoA-IV^{Q360H}, and apoA-IV^{T347S} proteins conjugated with C-terminal Alexa Fluor 488, or FITC, was separately examined by measuring steady-state fluorescence anisotropy (r) of Alexa Fluor 488 in PBS at 37 °C. The fluorescence anisotropy of conjugated apoA-IV depends on the ratio of the polarized excitation and emission light, and it is independent of the absolute emission intensity magnitudes (63, 74). To ensure the ruggedness of acquired polarization data, the fluorescence anisotropy experiments were repeated utilizing a Synergy Neo2 fluorimeter (BioTek). Using a pair of manual Cary Eclipse light polarizers, the polarized excitation (492 nm) and emission (517 nm) intensities at each titration point were measured, and the fluorescence anisotropy (r) values were quantified as we previously described (63, 69, 75).

Fluorescence quenching assays

The structural dynamics of apoA-IV variants was investigated exploiting the conformational change of N-terminal single tryptophan (W12) residue of apoA-IV polymorphisms in the presence and absence of DMPC. Tryptophan residues of

10 μM apoA-IV isoforms in 20 mM Hepes, pH 7.4, 140 mM NaCl were excited at 295 nm at 37 °C. The intrinsic fluorescence emission spectra of apoA-IV variants were recorded separately in a wavelength range of 300 to 500 nm in individual titrations with 8 M acrylamide and 8 M sodium iodide containing 1 μM $Na_2S_2O_3$. Equimolar concentrations of *N*-acetyl-L-tryptophanamide in the stated experimental conditions were used as control (40, 76). The maximum emission intensity change (ΔF) and wavelength shifts (Δλ) were monitored in triplicated experiments. The Stern–Volmer isotherms of the obtained maximum intensities were analyzed as a function of unbound to quenched apoA-IV (F_0/F) *versus* the total quencher concentration. The Stern–Volmer constants (K_{SV}) were quantified as previously described (75, 77–79).

FRET

Purified recombinant apoA-IV^{WT}, apoA-IV^{Q360H}, and apoA-IV^{T347S} proteins were separately conjugated with C-terminal Alexa Fluor 488 in one group (donor) and N-terminal Alexa Fluor 555 in another group (acceptor) in 20 mM HEPES buffer, pH 7.4, and 137 mM NaCl as described previously in the chemical modification section applying two FRET techniques: (i) C termini of two apoA-IV batches were labeled with a donor and an acceptor; (ii) C and N termini of two apoA-IV batches were labeled with a donor and an acceptor, respectively. Each sample was excited at 488 nm, and emission spectra were recorded in a wavelength range of 500 to 600 nm. The FRET efficiency (*E*) was calculated as $E = I_a / (I_d + I_a)$, where I_a is equal to the integrated fluorescence intensity of acceptor and I_d is the integrated fluorescence intensity of donor mixed with the acceptor. The intramolecular distance (*R*) between the C terminus of an apoA-IV molecule and N terminus of its homodimer was measured as $E = 1/[1 + (R/R_o)^6]$, where R_o is 70 Å Förster constant for the employed donor–acceptor fluorophores (79–81).

Thermal and chemical denaturation assays

Utilizing CD spectroscopy, the thermal denaturation assays were monitored from the change in molar ellipticity at 222 nm ($[\Theta]_{222}$) of apoA-IV variants (WT, Q360H, and T347S) over the temperature range of 25 to 75 °C at an increasing rate of 5 °C/min. Dichroic thermograms were subtracted from the corresponding PBS controls, averaged, and normalized. To quantify the thermal denaturation points (T_m), the first derivative of thermograms was plotted as a function of temperature (47, 82, 83). The thermal denaturation point of unconjugated purified (20 ± 1) μM apoA-IV variants in PBS were examined *via* intrinsic tryptophan excitation at 280 nm (84). Emission intensities were detected at (325 ± 0.1) nm as a function of temperature increase at 1 °C/min using 2-mm path length quartz cuvettes. The obtained emission intensities were averaged and normalized. To quantify the thermal denaturation points (T_m), the data were analyzed in a same manner as described previously for the dichroic thermograms (82, 83). The chemical denaturation assays of apoA-IV variants in PBS were examined from $[\Theta]_{222}$ change as a function of GuHCl in a concentration range from 0 to 2 M at 20 °C as previously described (39, 40, 47).

Dynamic light scattering

The R_h of the apoA-IV polymorphic isotypes were assessed through dynamic light scattering utilizing a DynaPro Plate Reader III (Wyatt) (47, 85). Minimum volume of 20 μl from purified recombinant apoA-IV variants, with a concentration of (20 ± 1) μM, was introduced into an opaque 384-well clear bottom plate (Corning) and examined at a constant temperature of 25 °C for 5 s/scan. The polydispersity properties of apoA-IV isotypes were determined by analyzing the accumulation of 10 to 15 trials using the Dynamics software package (47, 86, 87).

Isothermal titration calorimetry

Thermodynamics and binding parameters of apoA-IV variants were examined utilizing a MicroCal Auto-iTC200 instrument at 25 °C in PBS as we previously described (47, 69, 88). All experiments comprised of an initial delay of 60 s, first purge injection of 0.2 μl and subsequent 18 injections of 2 μl titrant, spaced every 180 s between every injection. The first point was removed from all datasets because of the difference in injection volume. For dissociation experiments, 40 μl of each apoA-IV variant solution were titrated into sample cell containing PBS. Fg titration experiments with apoA-IV^{WT}, apoA-IV^{Q360H}, and apoA-IV^{T347S} protein variants were individually performed with 2 μM apoA-IV variant in the sample cell and Fg (29 μM) as titrant. Fg titration experiments were analyzed with subtraction of the heat of dilution of the titrant. Acquired ITC data were analyzed using Origin 7.0 software (OriginLab) provided with the instrument employing the established methods (47, 75, 88, 89).

Computational modeling

Molecular models of full-length human apoA-IV^{WT}, apoA-IV^{Q360H}, and apoA-IV^{T347S} polymorphisms were computed utilizing a three-track neural network on Colab ProPlus as previously described (47, 90, 91). The generated secondary structure predictions with high confidence levels were refined and sorted based on the assessed accuracy scores. The structures of apoA-IV variants were compared with available crystal structure of dimeric apoA-IV^{WT} (Protein Data Bank code: 3S84) (10). The binding interfaces of apoA-IV variants with integrin αIIbβ3 headpiece (Protein Data Bank code: 3ZE2) (92) were examined utilizing a hybrid algorithm of template-based and *ab initio*–free model and analyzed in PyMol (Schrödinger) (73, 75, 93–95).

Statistical analysis

Data are presented as mean ± SD. Statistical significance was assessed by unpaired two-tailed Student's *t* test, one-way analysis of variance followed by Dunn's test for multiple paired comparisons using GraphPad 10 (Prism; GraphPad Software, Inc). A *p* Value <0.05 was considered statistically significant (47, 96).

Data availability

All data generated or analyzed during this study are included in this article (and its supporting information).

Supporting information—This article contains supporting information.

Acknowledgments—We acknowledge the Keenan Research Centre for Biomedical Science Core Facilities at St Michael's Hospital (Toronto, ON, Canada). We thank the Hospital for Sick Children (Toronto, ON, Canada) for the use of the Structural & Biophysical Core Facility. We also thank members of the Ni laboratory, the Johnson laboratory, and the Donaldson laboratory for the helpful discussions.

Author contributions—A. A. S., M. A. D. N., P. E. J., and H. N. conceptualization; A. A. S. methodology; A. A. S., S. S., V. P., and L. W. D. formal analysis; A. A. S., S. S., M. A. D. N., P. B., V. P., P. C., and L. W. D. investigation; L. W. D., P. E. J., and H. N. resources; A. A. S. writing–original draft; A. A. S., S. S., M. A. D. N., P. B., V. P., P. C., L. W. D., A. N. B., P. E. J., and H. N. writing–review & editing; A. A. S., S. S., and V. P. visualization; A. N. B. and P. E. J. supervision; L. W. D., A. N. B., P. E. J., and H. N. funding acquisition.

Funding and additional information—H. N. is funded by Heart and Stroke Foundation of Canada Grant-in-aid (grant no.: G-22-0031951) and Canadian Institutes of Health Research Foundation grant (grant no.: 389035). P. E. J. and L. W. D. are funded by Natural Sciences and Engineering Research Council of Canada Discovery grants. A. N. B. is funded by the Canadian Armed Forces , Surgeon General's Health Research Program. Canada. A. A. S. is a recipient of the Canadian Blood Services Centre for Innovation Postdoctoral Fellowship and Ontario Graduate Scholarship Awards (York University, Toronto). S. S. and M. A. D. N. are recipients of the Canadian Blood Services Centre for Innovation Postdoctoral Fellowship Awards. V. P. is a recipient of Canadian Institutes of Health Research Graduate Scholarship. The content is solely the responsibility of the authors and does not necessarily represent the official views of the funding agencies.

Conflict of interest—S. S., M. A. D. N., P. B., P. C., and H. N. were partially funded by CCOA Therapeutics, Inc. All other authors declare that they have no conflicts of interest with the contents of this article.

Abbreviations—The abbreviations used are: apoA-IV, apolipoprotein A-IV; BLI, biolayer interferometry; DMPC, 1,2-dimyristoyl-sn-glycero-3-phosphocholine; Fg, fibrinogen; GuHCl, guanidine chloride; HAS, human serum albumin; ITC, isothermal titration calorimetry; MALS, multiangle light scattering; Ni–NTA, nickel–nitrilotriacetic acid; SEC, size-exclusion chromatography.

References

1. Ponnuswamy, P., and Selvaraj, S. (1992) Structural similarities in the repeat sequences of plasma apolipoproteins, A-I, A-IV, and E. *Protein Seq. Data Anal.* **5**, 47–56
2. Wu, A. L., and Windmueller, H. G. (1978) Identification of circulating apolipoproteins synthesized by rat small intestine *in vivo*. *J. Biol. Chem.* **253**, 2525–2528
3. Utermann, G., and Beisiegel, U. (1979) Apolipoprotein A-IV: a protein occurring in human mesenteric lymph chylomicrons and free in plasma. *Eur. J. Biochem.* **99**, 333–344
4. Xu, X. R., Wang, Y., Adili, R., Ju, L., Spring, C. M., Jin, J. W., *et al.* (2018) Apolipoprotein A-IV binds αIIbβ3 integrin and inhibits thrombosis. *Nat. Commun.* **9**, 3608
5. Shoara, A. A., MacKeigan, D., Yu, S., Neves, M., Chen, P., Shen, C., *et al.* (2023) Structural analyses of apolipoprotein A-IV polymorphisms Q360H and T347S elucidate the inhibitory effect against thrombosis. *Res. Pract. Thromb. Haemost.* **7**, 15–16
6. Wang, F., Kohan, A. B., Kindel, T. L., Corbin, K. L., Nunemaker, C. S., Obici, S., *et al.* (2012) Apolipoprotein A-IV improves glucose homeostasis by enhancing insulin secretion. *Proc. Natl. Acad. Sci. U. S. A.* **109**, 9641–9646
7. Qu, J., Ko, C.-W., Tso, P., and Bhargava, A. (2019) Apolipoprotein A-IV: a multifunctional protein involved in protection against atherosclerosis and diabetes. *Cells*. https://doi.org/10.3390/cells8040319
8. Weinberg, R. B., Hopkins, R. A., and Jones, J. B. (1996) Purification, isoform characterization, and quantitation of human apolipoprotein A-IV. In **, 263**. *Methods in Enzymology*, Academic Press, Cambridge, MA: 282–296
9. Pearson, K., Saito, H., Woods, S. C., Lund-Katz, S., Tso, P., Phillips, M. C., *et al.* (2004) Structure of human apolipoprotein A-IV: a distinct domain architecture among exchangeable apolipoproteins with potential functional implications. *Biochemistry* **43**, 10719–10729
10. Deng, X., Morris, J., Dressmen, J., Tubb, M. R., Tso, P., Jerome, W. G., *et al.* (2012) The structure of dimeric apolipoprotein A-IV and its mechanism of self-association. *Structure* **20**, 767–779
11. Elshourbagy, N. A., Walker, D. W., Paik, Y. K., Boguski, M. S., Freeman, M., Gordon, J. I., *et al.* (1987) Structure and expression of the human apolipoprotein A-IV gene. *J. Biol. Chem.* **262**, 7973–7981
12. Lohse, P., Kindt, M. R., Rader, D. J., and Brewer, H. B. (1990) Genetic polymorphism of human plasma apolipoprotein A-IV is due to nucleotide substitutions in the apolipoprotein A-IV gene. *J. Biol. Chem.* **265**, 10061–10064
13. Gomaraschi, M., Putt, W. E., Pozzi, S., Iametti, S., Barbiroli, A., Bonomi, F., *et al.* (2010) Structure and function of the apoA-IV T347S and Q360H common variants. *Biochem. Biophys. Res. Commun.* **393**, 126–130
14. Lohse, P., Kindt, M. R., Rader, D. J., and Brewer, H. B. (1991) Three genetic variants of human plasma apolipoprotein A-IV. apoA-IV-1(Thr347—-Ser), apoA-IV-0(Lys167—-Glu,Gln360—-His), and apoA-IV-3(Glu165—-Lys). *J. Biol. Chem.* **266**, 13513–13518
15. Menzel, H.-J., Boerwinkle, E., Schrangl-Will, S., and Utermann, G. (1988) Human apolipoprotein A-IV polymorphism: frequency and effect on lipid and lipoprotein levels. *Hum. Genet.* **79**, 368–372
16. Wong, W. R., Hawe, E., Li, L. K., Miller, G. J., Nicaud, V., Pennacchio, L. A., *et al.* (2003) Apolipoprotein AIV gene variant S347 is associated with increased risk of coronary heart disease and lower plasma apolipoprotein AIV levels. *Circ. Res.* **92**, 969–975
17. Kretowski, A., Hokanson, J. E., McFann, K., Kinney, G. L., Snell-Bergeon, J. K., Maahs, D. M., *et al.* (2006) The apolipoprotein A-IV Gln360His polymorphism predicts progression of coronary artery calcification in patients with type 1 diabetes. *Diabetologia* **49**, 1946–1954
18. Kronenberg, F., Stühlinger, M., Trenkwalder, E., Geethanjali, F. S., Pachinger, O., von Eckardstein, A., *et al.* (2000) Low apolipoprotein A-IV plasma concentrations in men with coronary artery disease. *J. Am. Coll. Cardiol.* **36**, 751–757
19. Coller, B. S., and Shattil, S. J. (2008) The GPIIb/IIIa (integrin αIIbβ3) odyssey: a technology-driven saga of a receptor with twists, turns, and even a bend. *Blood* **112**, 3011–3025
20. Ruggeri, Z. M. (2002) Platelets in atherothrombosis. *Nat. Med.* **8**, 1227–1234
21. Zhu, G., Zhang, Q., Reddy, E. C., Carrim, N., Chen, Y., Xu, X. R., *et al.* (2017) The integrin PSI domain has an endogenous thiol isomerase function and is a novel target for antiplatelet therapy. *Blood* **129**, 1840–1854
22. Xu, X. R., Zhang, D., Oswald, B. E., Carrim, N., Wang, X., Hou, Y., *et al.* (2016) Platelets are versatile cells: new discoveries in hemostasis,

thrombosis, immune responses, tumor metastasis and beyond. *Crit. Rev. Clin. Lab. Sci.* **53**, 409–430
23. Murphy, A. J., Bijl, N., Yvan-Charvet, L., Welch, C. B., Bhagwat, N., Reheman, A., *et al.* (2013) Cholesterol efflux in megakaryocyte progenitors suppresses platelet production and thrombocytosis. *Nat. Med.* **19**, 586–594
24. Prifti, V., Shoara, A. A., Gallant, R. C., Slavkovic, S., Singh, K., Rand, M., *et al.* (2024) Novel mechanism of thrombosis and hemostasis involving platelet Alpha-dystroglycan. *Am. J. Hematol.* **100**, 101
25. Li, J., Karakas, D., Xue, F., Chen, Y., Zhu, G., Yucel, Y. H., *et al.* (2023) Desialylated platelet clearance in the liver is a novel mechanism of systemic immunosuppression. *Research* **6**, 0236
26. Karakas, D., and Ni, H. (2024) Unveiling platelets as immune regulatory cells. *Circ. Res.* **134**, 987–989
27. Hodivala-Dilke, K. M., McHugh, K. P., Tsakiris, D. A., Rayburn, H., Crowley, D., Ullman-Culleré, M., *et al.* (1999) β3-integrin–deficient mice are a model for Glanzmann thrombasthenia showing placental defects and reduced survival. *J. Clin. Invest.* **103**, 229–238
28. Yang, H., Reheman, A., Chen, P., Zhu, G., Hynes, R. O., Freedman, J., *et al.* (2006) Fibrinogen and von Willebrand factor-independent platelet aggregation *in vitro* and *in vivo*. *J. Thromb. Haemost.* **4**, 2230–2237
29. Phillips, D. R., Charo, I. F., and Scarborough, R. M. (1991) GPIIb-IIIa: the responsive integrin. *Cell* **65**, 359–362
30. Rao, L. V. M., and Pendurthi, U. R. (2012) Regulation of tissue factor coagulant activity on cell surfaces. *J. Thromb. Haemost.* **10**, 2242–2253
31. Smith, S. A., Travers, R. J., and Morrissey, J. H. (2015) How it all starts: initiation of the clotting cascade. *Crit. Rev. Biochem. Mol. Biol.* **50**, 326–336
32. Roberts, H. R. H., Maureane, M., and Dougald, M. (2006) A cell-based model of thrombin generation. *Semin. Thromb. Hemost.* **32**, 032–038
33. Ni, H., Denis, C. V., Subbarao, S., Degen, J. L., Sato, T. N., Hynes, R. O., *et al.* (2000) Persistence of platelet thrombus formation in arterioles of mice lacking both von Willebrand factor and fibrinogen. *J. Clin. Invest.* **106**, 385–392
34. Reheman, A., Yang, H., Zhu, G., Jin, W., He, F., Spring, C. M., *et al.* (2009) Plasma fibronectin depletion enhances platelet aggregation and thrombus formation in mice lacking fibrinogen and von Willebrand factor. *Blood* **113**, 1809–1817
35. Reheman, A., Tasneem, S., Ni, H., and Hayward, C. P. M. (2010) Mice with deleted multimerin 1 and α-synuclein genes have impaired platelet adhesion and impaired thrombus formation that is corrected by multimerin 1. *Thromb. Res.* **125**, e177–e183
36. Williams, S. C., Bruckheimer, S. M., Lusis, A. J., LeBoeuf, R. C., and Kinniburgh, A. J. (1986) Mouse apolipoprotein A-IV gene: nucleotide sequence and induction by a high-lipid diet. *Mol. Cell Biol.* **6**, 3807–3814
37. Deng, X., Walker, R. G., Morris, J., Davidson, W. S., and Thompson, T. B. (2015) Role of conserved proline residues in human apolipoprotein A-IV structure and function. *J. Biol. Chem.* **290**, 10689–10702
38. Haley, K. M., Loren, C. P., Phillips, K. G., and McCarty, O. J. T. (2011) Characterization of single platelet mass, volume, and density in response to agonist stimulation. *Blood* **118**, 5261
39. Dvorin, E., Mantulin, W. W., Rohde, M. F., Gotto, A. M., Pownall, H. J., and Sherrill, B. C. (1985) Conformational properties of human and rat apolipoprotein A-IV. *J. Lipid Res.* **26**, 38–46
40. Weinberg, R. B., Jordan, M. K., and Steinmetz, A. (1990) Distinctive structure and function of human apolipoprotein variant ApoA-IV-2. *J. Biol. Chem.* **265**, 18372–18378
41. Narayanaswami, V., Kiss, R. S., and Weers, P. M. M. (2010) The helix bundle: a reversible lipid binding motif. *Comp. Biochem. Physiol. A. Mol. Integr. Physiol.* **155**, 123–133
42. Record, M. T., Anderson, C. F., and Lohman, T. M. (1978) Thermodynamic analysis of ion effects on the binding and conformational equilibria of proteins and nucleic acids: the roles of ion association or release, screening, and ion effects on water activity. *Q. Rev. Biophys.* **11**, 103–178
43. Ohtori, N., Kondo, Y., and Ishii, Y. (2020) Molecular size and shape effects: rotational diffusion and the Stokes-Einstein-Debye relation. *J. Mol. Liq.* **314**, 113764
44. Duverger, N., Murry-Brelier, A., Latta, M., Reboul, S., Castro, G., Mayaux, J.-F., *et al.* (1991) Functional characterization of human recombinant apolipoprotein AIV produced in Escherichia coli. *Eur. J. Biochem.* **201**, 373–383
45. MacKeigan, D. T., Yu, S.-Y., Chazot, N., Zhang, D., Khoury, C. J., Lei, X., *et al.* (2024) Apolipoprotein A-IV polymorphisms Q360H and T347S attenuate its endogenous inhibition of thrombosis. *Biochem. Biophys. Res. Commun.* **712–713**, 149946
46. Wang, Y., Reheman, A., Spring, C. M., Kalantari, J., Marshall, A. H., Wolberg, A. S., *et al.* (2014) Plasma fibronectin supports hemostasis and regulates thrombosis. *J. Clin. Invest.* **124**, 4281–4293
47. Shoara, A. A., Singh, K., Peng, H. T., Moes, K., Yoo, J.-A., Sohrabipour, S., *et al.* (2025) Freeze-dried plasma: hemostasis and biophysical analyses for damage control resuscitation. *Transfusion*. https://doi.org/10.1111/trf.18124
48. Xu, R.-G., Gauer, J. S., Baker, S. R., Slater, A., Martin, E. M., McPherson, H. R., *et al.* (2021) GPVI (Glycoprotein VI) interaction with fibrinogen is mediated by avidity and the fibrinogen αc-region. *Arterioscler. Thromb. Vasc. Biol.* **41**, 1092–1104
49. Salonen, E. M., Jauhiainen, M., Zardi, L., Vaheri, A., and Ehnholm, C. (1989) Lipoprotein(a) binds to fibronectin and has serine proteinase activity capable of cleaving it. *EMBO J.* **8**, 4035–4040
50. Tsurupa, G., Ho-Tin-Noé, B., Anglés-Cano, E., and Medved, L. (2003) Identification and characterization of novel lysine-independent apolipoprotein(a)-binding sites in fibrin(ogen) αC-domains. *J. Biol. Chem.* **278**, 37154–37159
51. Tavoosi, N., Davis-Harrison, R. L., Pogorelov, T. V., Ohkubo, Y. Z., Arcario, M. J., Clay, M. C., *et al.* (2011) Molecular determinants of phospholipid Synergy in blood clotting. *J. Biol. Chem.* **286**, 23247–23253
52. Chinnaraj, M., Planer, W., and Pozzi, N. (2018) Structure of coagulation factor II: molecular mechanism of thrombin generation and development of next-generation anticoagulants. *Front. Med.* **5**, 281
53. Spronk, H. M. H., ten Cate, H., and van der Meijden, P. E. J. (2014) Differential roles of tissue factor and phosphatidylserine in activation of coagulation. *Thromb. Res.* **133**, S54–S56
54. Bakirova, D. R., Faizullin, D. A., Valiullina, Y. A., Salnikov, V. V., and Zuev, Y. F. (2017) Effect of lipid surface composition on the formation and structure of fibrin clots. *Bull. Exp. Biol. Med.* **163**, 722–725
55. Luchini, A., Tidemand, F. G., Araya-Secchi, R., Campana, M., Cárdenas, M., and Arleth, L. (2022) Structural model of tissue factor (TF) and TF-factor VIIa complex in a lipid membrane: a combined experimental and computational study. *J. Colloid Interf. Sci.* **623**, 294–305
56. Dahlbäck, B. (2008) Advances in understanding pathogenic mechanisms of thrombophilic disorders. *Blood* **112**, 19–27
57. Mei, X., and Atkinson, D. (2011) Crystal structure of C-terminal truncated apolipoprotein A-I reveals the assembly of high density lipoprotein (HDL) by dimerization. *J. Biol. Chem.* **286**, 38570–38582
58. Micsonai, A., Moussong, É., Wien, F., Boros, E., Vadászi, H., Murvai, N., *et al.* (2022) BeStSel: webserver for secondary structure and fold prediction for protein CD spectroscopy. *Nucleic Acids Res.* **50**, W90–W98
59. Boodram, S. N., Cho, C. M., Tavares, T. J., and Johnson, P. E. (2011) Identification of RNA–ligand interactions by affinity electrophoresis. *Anal. Biochem.* **409**, 54–58
60. Kwan, J. J., Slavkovic, S., Piazza, M., Wang, D., Dieckmann, T., Johnson, P. E., *et al.* (2020) HACS1 signaling adaptor protein recognizes a motif in the paired immunoglobulin receptor B cytoplasmic domain. *Commun. Biol.* **3**, 672
61. Neves, M. A. D., Slavkovic, S., Reinstein, O., Shoara, A. A., and Johnson, P. E. (2019) A proof of concept application of aptachain: ligand-induced self-assembly of a DNA aptamer. *RSC Adv.* **9**, 1690–1695
62. Tong, J., Nejman-Faleńczyk, B., Bloch, S., Węgrzyn, A., Węgrzyn, G., and Donaldson, L. W. (2020) Ea22 proteins from lambda and shiga toxin-producing bacteriophages balance structural diversity with functional similarity. *ACS Omega* **5**, 12236–12244
63. Shoara, A. A., Churcher, Z. R., Steele, T. W. J. J., and Johnson, P. E. (2020) Analysis of the role played by ligand-induced folding of the cocaine-binding aptamer in the photochrome aptamer switch assay. *Talanta.* **217**, 121022

64. Hermanson, G. T. (2013) Chapter 10 - Fluorescent probes. In *Bioconjugate Techniques*, 3rd Ed., Academic Press, Boston: 395–463. https://doi.org/10.1016/B978-0-12-382239-0.00010-8
65. Shen, C., MacKeigan, D. T., Shoara, A. A., Xu, R., Bhoria, P., Karakas, D., *et al.* (2023) Dual roles of fucoidan-GPIbα interaction in thrombosis and hemostasis: implications for drug development targeting GPIbα. *J. Thromb. Haemost.* **21**, 1274–1288
66. Staros, J. V. (1982) N-hydroxysulfosuccinimide active esters: bis(N-hydroxysulfosuccinimide) esters of two dicarboxylic acids are hydrophilic, membrane-impermeant, protein cross-linkers. *Biochemistry* **21**, 3950–3955
67. Gidley, G. N., Holle, L. A., Burthem, J., Bolton-Maggs, P. H. B., Lin, F.-C., and Wolberg, A. S. (2018) Abnormal plasma clot formation and fibrinolysis reveal bleeding tendency in patients with partial factor XI deficiency. *Blood Adv.* **2**, 1076–1088
68. Ciesielski, G. L., Hytönen, V. P., and Kaguni, L. S. (2016) Biolayer interferometry: a novel method to elucidate protein–protein and protein–DNA interactions in the mitochondrial DNA replisome. In: McKenzie, M., ed. *Mitochondrial DNA: Methods and Protocols*, 231, Springer, New York, NY: 223. https://doi.org/10.1007/978-1-4939-3040-1_17
69. Ma, X., Liang, J., Zhu, G., Bhoria, P., Shoara, A. A., MacKeigan, D. T., *et al.* (2023) SARS-CoV-2 RBD and its variants can induce platelet activation and clearance: implications for antibody therapy and vaccinations against COVID-19. *Research* **6**, 0124
70. Tubb, M. R., Silva, R. A. G. D., Pearson, K. J., Tso, P., Liu, M., and Davidson, W. S. (2007) Modulation of apolipoprotein A-IV lipid binding by an interaction between the N and C termini. *J. Biol. Chem.* **282**, 28385–28394
71. Donaldson, L. W., Wojtyra, U., and Houry, W. A. (2003) Solution structure of the dimeric zinc binding domain of the chaperone ClpX. *J. Biol. Chem.* **278**, 48991–48996
72. Micsonai, A., Wien, F., Kernya, L., Lee, Y.-H., Goto, Y., Réfrégiers, M., *et al.* (2015) Accurate secondary structure prediction and fold recognition for circular dichroism spectroscopy. *Proc. Natl. Acad. Sci. U. S. A.* **112**, E3095–E3103
73. Kaiyum, Y. A., Hoi Pui Chao, E., Dhar, L., Shoara, A. A., Nguyen, M.-D., Mackereth, C. D., *et al.* (2024) Ligand-induced folding in a dopamine-binding DNA aptamer. *ChemBioChem.* **25**, e202400493
74. LeTilly, V., and Royer, C. A. (1993) Fluorescence anisotropy assays implicate protein-protein interactions in regulating trp repressor DNA binding. *Biochemistry* **32**, 7753–7758
75. Slavkovic, S., Shoara, A. A., Kaiyum, Y. A., Churcher, Z. R., Liu, T., Simine, L., *et al.* (2024) Amodiaquine nonspecifically binds double stranded and three-way Junction DNA structures. *ChemBioChem* **25**, e202400116
76. Ghiron, C. A., and Longworth, J. W. (1979) Transfer of singlet energy within trypsin. *Biochemistry* **18**, 3828–3832
77. Shoara, A. A., Slavkovic, S., Donaldson, L. W., and Johnson, P. E. (2017) Analysis of the interaction between the cocaine-binding aptamer and its ligands using fluorescence spectroscopy. *Can. J. Chem.* **95**, 1253–1260
78. Mocz, G., and Ross, J. A. (2013) Fluorescence techniques in analysis of protein–ligand interactions. In: Williams, M. A., Daviter, T., eds. *Protein-Ligand Interactions: Methods and Applications*, Humana Press, Totowa, NJ: 169–210. https://doi.org/10.1007/978-1-62703-398-5_7
79. Shoara, A. A., Churcher, Z. R., Slavkovic, S., and Johnson, P. E. (2021) Weak binding of levamisole by the cocaine-binding aptamer does not interfere with an aptamer-based detection assay. *ACS Omega* **6**, 24209–24217
80. Clegg, R. M. (1995) Fluorescence resonance energy transfer. *Curr. Opin. Biotechnol.* **6**, 103–110
81. Börjesson, K., Preus, S., El-Sagheer, A. H., Brown, T., Albinsson, B., and Wilhelmsson, L. M. (2009) Nucleic acid base analog FRET-pair facilitating detailed structural measurements in nucleic acid containing systems. *J. Am. Chem. Soc.* **131**, 4288–4293
82. Shoara, A. A., Reinstein, O., Borhani, O. A., Martin, T. R., Slavkovic, S., Churcher, Z. R., *et al.* (2018) Development of a thermal-stable structure-switching cocaine-binding aptamer. *Biochimie* **145**, 137–144
83. Neves, M. A. D., Shoara, A. A., Reinstein, O., Abbasi Borhani, O., Martin, T. R., and Johnson, P. E. (2017) Optimizing stem length to improve ligand selectivity in a structure-switching cocaine-binding aptamer. *ACS Sens.* **2**, 1539–1545
84. Weinberg, R. B. (1988) Exposure and electronic interaction of tyrosine and tryptophan residues in human apolipoprotein A-IV. *Biochemistry* **27**, 1515–1521
85. Harkness, R. W., Ripstein, Z. A., Di Trani, J. M., and Kay, L. E. (2023) Flexible client-dependent cages in the assembly landscape of the periplasmic protease-chaperone DegP. *J. Am. Chem. Soc.* **145**, 13015–13026
86. Rujas, E., Kucharska, I., Tan, Y. Z., Benlekbir, S., Cui, H., Zhao, T., *et al.* (2021) Multivalency transforms SARS-CoV-2 antibodies into ultrapotent neutralizers. *Nat. Commun.* **12**, 3661
87. Harkness, R. W., Toyama, Y., Ripstein, Z. A., Zhao, H., Sever, A. I. M., Luan, Q., *et al.* (2021) Competing stress-dependent oligomerization pathways regulate self-assembly of the periplasmic protease-chaperone DegP. *Proc. Natl. Acad. Sci. U. S. A.* **118**, e2109732118
88. Slavkovic, S., and Johnson, P. E. (2023) Analysis of aptamer-small molecule binding interactions using isothermal titration calorimetry. In: Mayer, G., Menger, M. M., eds. *Nucleic Acid Aptamers: Selection, Characterization, and Application*, Springer US, New York, NY: 105–118. https://doi.org/10.1007/978-1-0716-2695-5_8
89. Freiburger, L. A., Auclair, K., and Mittermaier, A. K. (2009) Elucidating protein binding mechanisms by variable-c ITC. *ChemBioChem.* **10**, 2871–2873
90. Baek, M., DiMaio, F., Anishchenko, I., Dauparas, J., Ovchinnikov, S., Lee, G. R., *et al.* (2021) Accurate prediction of protein structures and interactions using a three-track neural network. *Science* **373**, 871–876
91. Mirdita, M., Schütze, K., Moriwaki, Y., Heo, L., Ovchinnikov, S., and Steinegger, M. (2022) ColabFold: making protein folding accessible to all. *Nat. Methods* **19**, 679–682
92. Zhu, J., Zhu, J., and Springer, T. A. (2013) Complete integrin headpiece opening in eight steps. *J. Cell Biol.* **201**, 1053–1068
93. Yan, Y., Wen, Z., Wang, X., and Huang, S.-Y. (2017) Addressing recent docking challenges: a hybrid strategy to integrate template-based and free protein-protein docking. *Proteins Struct. Funct. Bioinforma.* **85**, 497–512
94. Donaldson, L. W. (2021) Molecular modeling the proteins from the exoxis region of lambda and shigatoxigenic bacteriophages. *Antibiotics*. https://doi.org/10.3390/antibiotics10111282
95. Neves, M. A. D., Ni, T. T., MacKeigan, D. T., Shoara, A. A., Lei, X., Slavkovic, S., *et al.* (2024) Salvianolic acid B inhibits thrombosis and directly blocks the thrombin catalytic site. *Res. Pract. Thromb. Haemost.* **8**, 102443
96. Rao, T. N. (2018) Ch. 7 - validation of analytical methods. In: Stauffer, M. T., ed. *Calibration and Validation of Analytical Methods*, 41, IntechOpen, Rijeka: 131. https://doi.org/10.5772/intechopen.72087